Thesis for the degree of Doctor of Philosophy

Propulsion System Solutions for Future Fighter Aircraft Requirements

Daniel Rosell

Department of Mechanical Engineering
Division of Fluid Dynamics
CHALMERS UNIVERSITY OF TECHNOLOGY
Göteborg, Sweden 2026

Propulsion System Solutions for Future Fighter Aircraft Requirements
Daniel Rosell
ISBN 978-91-8103-405-9

Doktorsavhandlingar vid Chalmers tekniska högskola
Ny serie nr 5862
ISSN 0346-718X

Department of Mechanical Engineering
Division of Fluid Dynamics
Chalmers University of Technology
SE–412 96 Göteborg, Sweden
Telephone + 46 (0) 31 – 772 1000

Typeset by the author using LaTeX.

Printed by Chalmers Reproservice
Göteborg, Sweden 2026

To my family

Abstract

The requirements of military aircraft are becoming increasingly complex. In addition to traditional requirements such as high maneuverability and high supersonic speed capabilities, there is now a demand for large amounts of power extraction from different aircraft systems. Such systems produce excessive heat that must be dissipated. To meet all these needs, the aircraft engine will play a crucial role. This work has demonstrated how large power off-takes affect not only the engine but also the aircraft in different maneuvers of a typical fighter aircraft mission. Extracting large amounts of power from the engine limits the aircraft performance in challenging maneuvers and increases engine fuel consumption in different parts of the mission. In some parts of the flight envelope, the ability to extract large amounts of power can be significantly limited to ensure safe operation of the engine.

Variable cycle engines might offer improved operability, improved engine performance, and solutions to the thermal management problem. Alongside the conventional turbofan engine, a variable cycle concept was studied, in which an additional outer bypass stream was introduced. This bypass stream is maintained by a single-stage fan on blade, FLADE. The advantages of this concept, compared to more advanced architectures, are reduced complexity and weight. The analysis indicates that the concept has the potential to improve the subsonic cruise range and the loiter endurance of a fighter aircraft. Potential improvements and limitations have been evaluated for different throttle settings across the flight envelope of the aircraft.

Keywords: Fighter aircraft performance, engine performance, low bypass ratio, mixed flow, turbofan engine, power extraction, variable cycle engine

Acknowledgments

I am very grateful to my academic supervisor, Professor Tomas Grönstedt. His support includes everything from supervision, engine model development, and sharing his knowledge and ideas. I am also very thankful to my colleagues at Saab Aeronautics and particularly Michael Säterskog, Sebastian Arvidson, Hans Kling, Michael Newberry, Nor Al-Mosawi and Hans-Peter Magnusson who provided valuable technical and practical support throughout the project. I also acknowledge the work of Pedro David Bravo-Mosquera who provided a conceptual aircraft design for the engine performance study. Pedro's work was important to establish a use case and I appreciated our collaboration in the project.

This work has been funded by the Swedish Governmental Agency for Innovation Systems (VINNOVA) within the National Aviation Research Programme (NFFP diary number 2020-00690 and 2023-01181) and Saab Aeronautics.

Daniel Rosell
Linköping, June 2026

List of Publications

This thesis is based on the following papers:

Paper 1. Daniel Rosell and Tomas Grönstedt. *Design Considerations of Low Bypass Ratio Mixed Flow Turbofan Engines with Large Power Extraction.* Fluids 2022, 7(1), 21.

Paper 2. Daniel Rosell, Tomas Grönstedt, Pedro David Bravo-Mosquera, Fernando Martini Catalano. *Low BPR Turbofan Performance with Power Extraction.* 33rd Congress of the International Council of the Aeronautical Sciences, Stockholm, Sweden, 2022, 6, 4382.

Paper 3. Daniel Rosell, Tomas Grönstedt. *Aircraft Performance Impact with a Turbofan Engine Using a Fan on Blade.* Journal of Propulsion and Power, 2026, 42(3), 392.

Paper 4. Emil Ellenius, Tomas Grönstedt, Daniel Rosell. *Aerodynamic Design of Fan on Blade for Multiple Operating Points.* Submitted to The Aeronautical Journal, 2026.

Other relevant publications co-authored by Daniel Rosell:

Marcelo Assato, Ali Altar Incer, Lucilene Moraes, Jesuino Takachi Tomita, Cleverson Binghenti, Pedro Bravo-Mosquera, **Daniel Rosell**, Tomas Grönstedt. *Performance Benefits of a Fan on Blade - FLADE - For a Variable Cycle Engine.* 33rd Congress of the International Council of the Aeronautical Sciences, Stockholm, Sweden, 2022, 7, 4888.

Nomenclature

Abbreviations

A	–	area
A/B	–	afterburner
AC	–	alternating current
ACE	–	adaptive cycle engine
ACM	–	air cycle machine
AHP	–	auxiliary hydraulic pump
AMAD	–	airframe mounted accessory drive
AR	–	aspect ratio
A_c	–	capture area
APU	–	accessory power unit
ATS	–	air turbine starter
BPR	–	bypass ratio
C_D	–	drag coefficient
C_{D_0}	–	zero-lift drag coefficient
C_f	–	skin friction coefficient
C_{fe}	–	equivalent skin friction coefficient
C_L	–	lift coefficient
C_{L_α}	–	lift curve slope
$C_{L_{design}}$	–	design lift coefficient
C_{TO}	–	corrected power take-off
c_p	–	specific heat at constant pressure
D	–	drag
D	–	diameter
DC	–	direct current
D_{aft}	–	afterbody drag
D_{spill}	–	spillage drag
E	–	endurance
E_s	–	specific endurance
E_{WD}	–	wave-drag efficiency factor
ECS	–	environmental control system
EHP	–	electrical hydraulic pump
EMAD	–	engine mounted accessory drive

F	–	force
FADEC	–	full authority digital engine control
F_G	–	Installed gross thrust
F_N	–	Installed net thrust
FLADE	–	fan on blade
FPR	–	fan pressure ratio
f_s	–	fuel specific energy
f	–	friction coefficient
GESTPAN	–	general stationary and transient propulsion analysis
HP	–	high-pressure
HPC	–	high-pressure compressor
HPCPR	–	high-pressure compressor pressure ratio
HPT	–	high-pressure turbine
IGV	–	inlet guide vane
h	–	enthalpy
h	–	altitude
h_e	–	specific energy
K	–	drag due to lift factor
K_{100}	–	drag due to lift factor with 100 % leading-edge suction
K_0	–	drag due to lift factor with 0 % leading-edge suction
k	–	skin roughness value
L	–	lift
L/D	–	lift-to-drag ratio
LP	–	low-pressure
LPC	–	low-pressure compressor
LPT	–	low-pressure turbine
l	–	characteristic length
M	–	Mach number
M_{DD}	–	drag-divergent Mach number
MFR	–	mass flow ratio
MHP	–	mechanical hydraulic pump
MIL	–	military power (maximum non-augmented power)
MAX	–	maximum augmented power (A/B in operation)
$\dot{m}$	–	mass flow
N	–	rotational speed
N_1	–	fan rotational speed
N_{1c}	–	corrected fan speed
N_2	–	core rotational speed
n_e	–	number of engines
OPR	–	overall pressure ratio, also referred to as π_c

P	–	power
P_s	–	specific power
P_{TO}	–	absolute power take-off
P_{cTO}	–	absolute power take-off
PTS	–	power transmission shaft
p	–	pressure
p_0	–	stagnation pressure
q	–	dynamic pressure
R	–	range
R_s	–	specific range
Re	–	Reynold's number
Re_{cutoff}	–	cutoff Reynold's number
S	–	leading-edge suction parameter
SFC	–	specific fuel consumption
SLS	–	sea level static
S_{ref}	–	wing reference area
S_{wet}	–	aircraft wetted area
SLS	–	sea level static
T	–	temperature
T_{std}	–	sea level static temperature of the standard atmosphere
T	–	installed thrust
T_0	–	stagnation temperature
T_e	–	installed thrust per engine
$TSFC$	–	installed thrust specific fuel consumption
TB	–	thermal battery
TR	–	throttle ratio
TRU	–	transformer rectifying unit
T/W	–	thrust-to-weight ratio
$(T/W)_{TO}$	–	take-off thrust-to-weight ratio
V	–	velocity
V_G	–	ground speed
V_∞	–	true air speed
VCE	–	variable cycle engine
W	–	weight
W_e	–	empty weight
W_p	–	payload weight
W_{TO}	–	take-off weight
$WEICO$	–	weight and cost estimation
W/S	–	wing loading
$(W/S)_{TO}$	–	take-off wing loading

Greek

α	–	bypass ratio
α_{fan}	–	fan bypass ratio, FLADE flow to turbofan flow ratio
α_{core}	–	core bypass ratio, bypass flow to core flow ratio
α_{shock}	–	ratio of intake supersonic loss to normal shock loss
α_{spill}	–	spillage drag to pre-entry drag ratio
β	–	aircraft weight fraction relative to takeoff weight
β_f	–	fuel schedule factor, off-design fuel flow relative to the design point fuel flow
β_{fan}	–	operating line offset in fan map
β_{HPC}	–	operating line offset in HPC map
η	–	efficiency
η_{th}	–	thermal efficiency
η_p	–	propulsive efficiency
η_p	–	pressure recovery
γ	–	aircraft climb angle
γ	–	ratio of specific heats
δ	–	non-dimensional pressure (p/p_{SLS})
δ_0	–	non-dimensional stagnation pressure (p_0/p_{SLS})
ϵ	–	thrust inclination angle compared to free stream
π	–	pressure ratio
π_f	–	fan pressure ratio
π_c	–	overall pressure ratio, also referred to as OPR
θ	–	non-dimensional temperature (T/T_{std})
θ_0	–	non-dimensional stagnation temperature (T_0/T_{std})
$\theta_{0,break}$	–	theta break, θ_0 where the engine is operating at OPR_{max} and $T_{4,max}$
Λ	–	sweep
Λ_{LE}	–	leading-edge sweep
μ	–	viscosity
ρ	–	density
τ_w	–	frictional shear stress

Subscripts

0	–	stagnation
1	–	air intake
1	–	duct inlet
2	–	fan inlet
2	–	duct outlet
3	–	high-pressure compressor delivery
4	–	high-pressure turbine inlet
5	–	low-pressure turbine exit
6	–	front face of afterburner
7	–	nozzle inlet
8	–	nozzle throat
9	–	nozzle exit
∞	–	free-stream
a	–	air
c	–	conditions at entry (of intake)
c	–	compression
c	–	corrected
f	–	fan
max	–	maximum value (T_4, OPR)
pre	–	pre-entry
std	–	standard sea level static conditions
x	–	velocity direction
z	–	direction perpendicular to the velocity direction

Contents

Part I

Introductory chapters

Chapter 1

Introduction

1.1 Background

The requirements for fighter aircraft are becoming more and more extensive. The ability of aircraft to perform increasingly advanced maneuvers has been a driving force for aircraft and engine design over the past century. Nowadays, these performance requirements are accompanied by demands for reduced radar and infrared (IR) signature [1–3], requirements that quite often have adverse effects on the above-mentioned performance requirements [4]. In addition, more advanced equipment that requires large amounts of electrical power is introduced in modern fighter aircraft [5]. All of this affects the aircraft engine in different ways. Although pure performance requirements such as maximum speed and altitude have recently been considered less significant, or at least have been compromised in view of the new requirements that have arisen in recent years [1], the high T/W ratio for newly developed fighters [6] shows that the performance of the aircraft is still of great importance [3].

Figure 1.1: Takeoff of the Gripen E fighter.

Sizing a conventional turbofan engine for requirements of high maneuverability and high supersonic speed leads to greater thrust variation over a mission and that the engine is oversized for flight cases such as cruise and loiter, where the

thrust requirement is low. This causes installation losses to increase in these flight cases [4, 7, 8]. Traditionally, variable geometry intakes have been used to reduce these losses, but the disadvantage is that such intakes are both heavier and more complex [9–13]. For a fighter aircraft with a traditional fighter mission, spending most of its time in subsonic cruise and loiter, this may prove to be a too high price to pay for the short-duration improved high-speed performance [12].

Engine intake and exhaust may need to be designed to reduce radar and IR signature, which, in turn, can have consequences in terms of engine distortion and performance [2, 4] Large amounts of power off-takes from the aircraft engine have both direct and indirect effects on the engine. The direct effects concern engine performance and operability [14, 15], while the indirect effects relate to the excessive heat generated by power-consuming equipment [16, 17]. The engine architecture and its integration into the aircraft may play a key role in dissipating this excessive heat from the aircraft.

Power is traditionally consumed by pumps and systems for hydraulic, pneumatic, and control [14, 18]. Added to this is a constantly increasing need for new power-requiring equipment such as radars and mission systems [5]. Furthermore, this power requirement has changed in the sense that mechanical systems are gradually being replaced by electrical ones. Mechanical control systems have been replaced by electrical control systems, such as fly-by-wire for flight control and full authority digital engine control (FADEC) for engine control [19]. Hydraulic systems are about to be replaced by electric machinery [19–23]. Figure 1.2 [24] gives an overview of the Gripen fighter vehicle system.

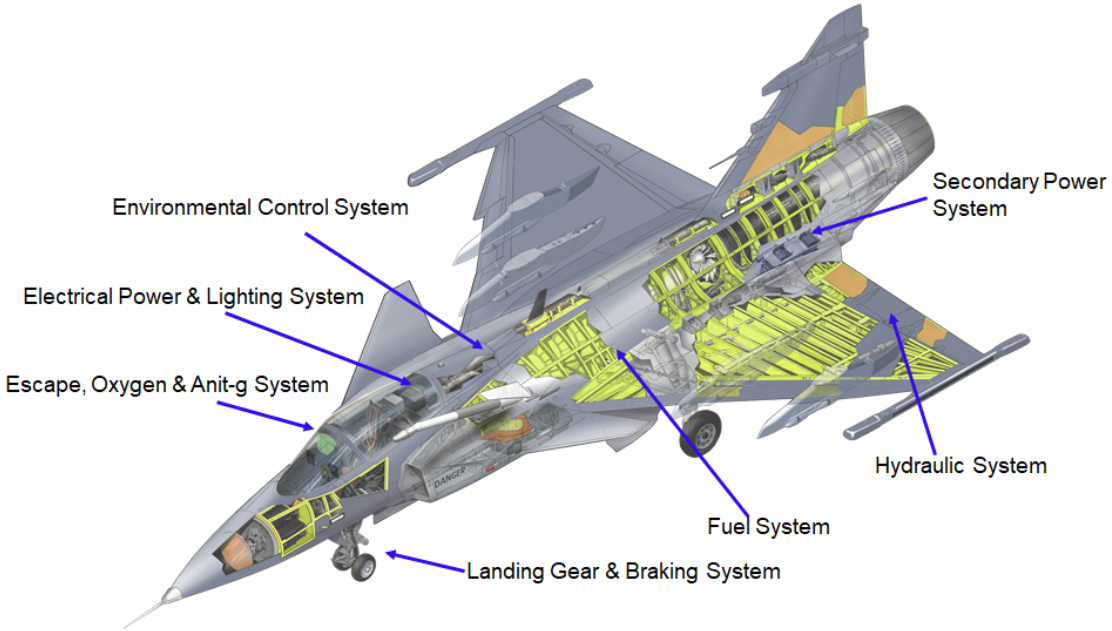

Figure 1.2: The Gripen aircraft vehicle systems as illustrated in [24].

A typical aircraft power flow system is illustrated in Figure 1.3 [25, 26]. The power supply to the aircraft's electrical and hydraulic systems is provided by an

airframe mounted accessory drive (AMAD). AMAD power is provided by the aircraft engine through an engine-mounted accessory drive (EMAD) and a power transmission shaft (PTS). The accessory drives contribute to the aircraft cross-sectional area and thus increase the drag of the aircraft, especially during supersonic flight [27–29]. Therefore, it has long been discussed whether these units could be replaced by a generator directly connected to the aircraft engine, which provides the aircraft with all the required power [30, 31]. However, such a solution is accompanied by technical challenges such as high ambient operating temperatures, possible increase in the volume and weight of components, difficulties in accessing the equipment to perform maintenance, and the need to completely electrically power the engine accessories [30, 31].

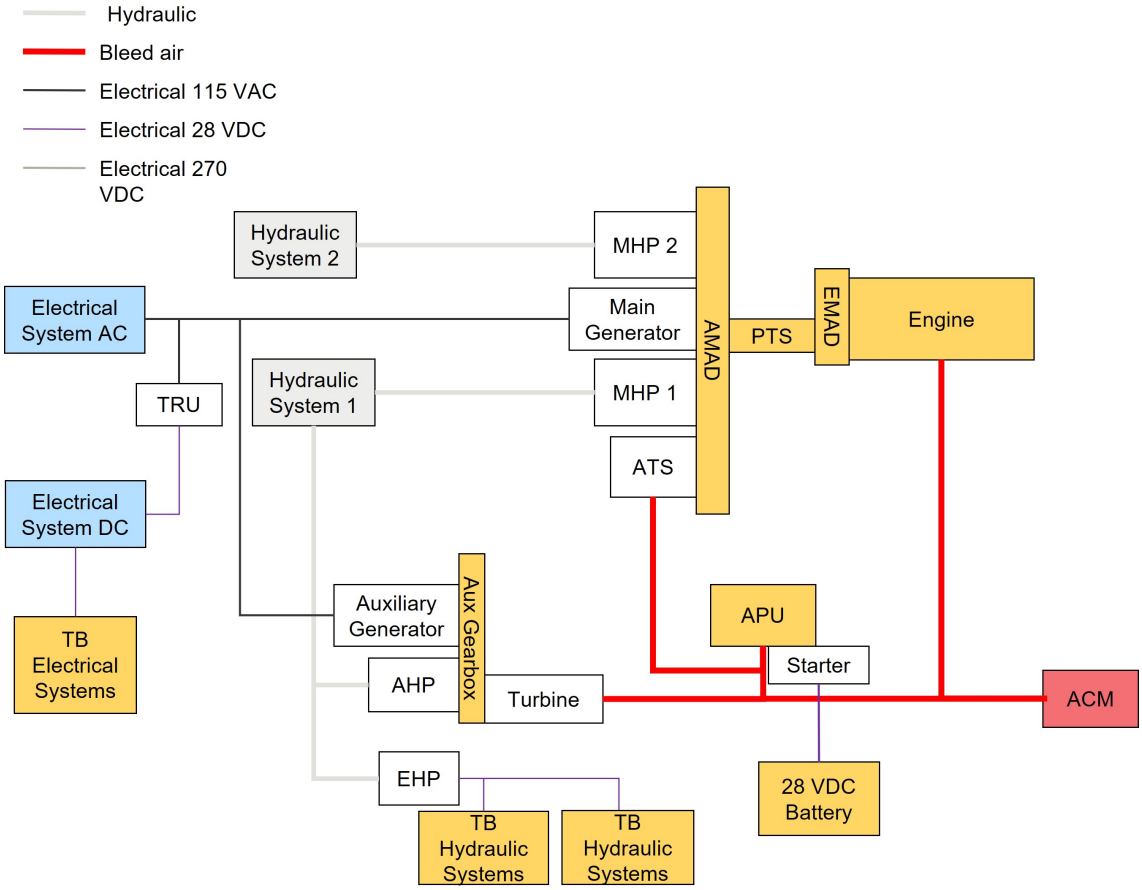

Figure 1.3: Power system of a typical aircraft [25, 26].

A major part of the work focused on the performance impact of large power extraction on a twin-spool low-bypass-ratio mixed-flow turbofan engine. This is the engine type most commonly used in fighter aircraft today. Large power extraction has previously been studied for high-bypass-ratio turbofan engines, either from a performance point of view [32–34] or from an operability perspective [32–35]. This work has identified similar performance characteristics for low-bypass turbofan engines, although these engines differ both in terms of design and mission requirements. The mission itself and its various phases have proven to be significant in influencing

performance as the engine is limited in different ways in different parts of the mission. This means that it may be more or less beneficial to extract power in different parts of the mission, but also that the most favorable shaft (HP or LP) for power extraction varies from one mission phase to the other. In Chapter 4 this is illustrated both with regard to engine performance and from an aircraft performance perspective. Although these results demonstrate good potential for power off-take in different parts of a fighter mission, a conventional turbofan engine also has limitations on how much power that can be extracted, for instance from an operability point of view. In this perspective, modern types of variable cycle engines (VCE) become interesting, with their inherent flexibility to extract large amounts of power [36] and also providing an additional bypass stream for cooling [37]. These features, combined with the performance advantages traditionally attributed to VCEs, make them an interesting option for the next generation of fighter aircraft.

What truly motivates VCEs is their ability to combine high maximum performance during demanding maneuvers with low fuel consumption during flight conditions, such as cruise and loiter [38]. A conventional turbofan engine with high thrust capability exhibits reduced fuel efficiency at part-power due to high installation losses [7]. VCEs combine high specific thrust in demanding maneuvers with improved fuel efficiency in phases with low thrust requirements, by maintaining a higher airflow at part-power [39]. In this way, the propulsive efficiency of the engine can be improved and spillage drag can be reduced. However, for a VCE to be justified, these advantages must outweigh disadvantages such as increased weight and complexity [40, 41].

A relatively simple variable cycle engine was studied. It uses a fan tip on blade (FLADE) component to establish an outer bypass stream on a conventional low-bypass-ratio turbofan engine. In this way, it enables many of the advantages of more advanced VCEs, without the latter's extensive changes to the turbofan engine design and control. This concept, here referred to as FLADE turbofan, has been studied in [42–46], but less extensive in terms of engine and aircraft performance or with a different focus. This thesis consists of two main parts. In the first part, an introduction to the research field is given, describing the work that has been carried out and the results that have been achieved. The research papers are appended in the second part.

1.2 Method

The analyses were carried out for a fighter mission and for a conceptual aircraft design that was provided by the University of São Paulo. The aircraft thrust requirements and weight fractions in different parts of the fighter mission have been used to size the different engines that were used for engine performance analysis. An aircraft performance tool has been developed to study the impact of various engine architectures on aircraft performance, not only in different parts of the fighter mission, but also over the entire flight envelope. The Chalmers in-house tool GESTPAN (general stationary and transient propulsion analysis) [38] has been used to model a low-bypass-ratio turbofan engine and a FLADE turbofan engine. The characteristics of different thermodynamic cycles and their impact on aircraft and engine performance

have been studied. Aircraft performance is evaluated throughout the flight envelope with input from thousands of engine off-design simulations. Processing such a huge amount of data required the development of a MATLAB tool to initiate and run GESTPAN simulations, and to store and to post-process the simulation results. This initiating and post-processing tool consists of about 250 scripts and functions. A comprehensive performance data collection has been gathered for each engine concept that has been studied, which contains engine performance for different combinations of altitude and Mach number with varying thrust levels. These performance data are matched with the aircraft thrust requirement in different phases of the aircraft mission and at each point of the flight envelope for a certain aircraft weight. A tool developed by Chalmers in collaboration with Stuttgart University has been used for conceptual engine design and weight estimation [47].

1.3 Limitations

This work has mainly focused on engine performance in steady state operation. Engine transients were not considered in the performance analysis. Operability issues such as engine surge, which are typically transient phenomena, have not been studied in depth either. The evaluation here is limited to studying the operating points within the compressor maps in on-design and off-design conditions in steady-state operating conditions to ensure adequate margins for surge and choking. The omission of engine transients in the analysis of aircraft performance may appear to be a major limitation, but this is not really the case. In the aircraft maneuvers being studied, the engine acceleration time constitutes only a small part of the aircraft's acceleration time, and it is reasonable to assume a constant maximum thrust throughout the entire maneuver. Thermal transients impact radial and axial clearances, variable geometries, and aerodynamic matching of components, which has some impact on engine performance [48], but it is not within the scope of this work to quantify its impact on maximum performance. Moreover, it is not an unreasonable assumption that the engine enters these maneuvers with a high initial engine temperature. For example, the analyzed acceleration phase follows directly on the combat phase, in which the engine is already operating at its maximum inlet temperature.

Extracting large amounts of power from a turbofan engine entails challenges, not only from a performance perspective but also from an operability and design perspective. These challenges become increasingly demanding at higher altitudes and lower flight velocities [15]. If, for instance, large amounts of power are extracted from the HP shaft, it leads to reduced surge margins. Large amounts of power extraction from the LP shaft may require a HPC overspeed margin to avoid considerable thrust reductions [29]. The pure performance analysis also does not take into account possible practical considerations in choosing one shaft for power extraction over the other. Such factors could be accessibility and maintenance facilitation. Other factors that have traditionally been in favor of extracting power from the HP shaft are the shaft operating speed and the shaft speed variations under the various operating conditions of the engine [31]. The HP shaft speed is higher and the shaft speed fluctuations are more moderate compared to the speeds of the LP shaft.

Engine off design simulations are restricted by the limit maximum overall pressure ratio π_c or the maximum turbine inlet temperature, T_4 [49]. This control concept provides a good description of typical engine control, although it is a simplification. In some parts of the flight envelope, the engine may be further limited by other restrictions such as the maximum compressor discharge temperature T_3 or pressure P_3, the maximum fan speed N_1, or the maximum core speed N_2 [7, 15, 50].

The project work has been carried out as an engine reengineering study for an already existing aircraft, where the conceptual design of the aircraft, which was presented in [51], has been largely unchanged. This has been done with the main purpose of studying the impact of different engine concepts, various choices of thermodynamic cycles, and requirements for large power off-takes on aircraft capabilities. The design process of a completely new aircraft is otherwise an iterative process in which any improvement or deterioration compared to previous estimates has consequences for the design of the aircraft [49, 52].

The aircraft performance tool, which is described in Section 2.2, uses available low-fidelity models and empirical methods from public sources to estimate the aerodynamics of the fighter aircraft based on the geometric data provided for the aircraft, and typical characteristics of fighter aircraft [52–54]. The use of such methods is common practice in the conceptual design phase [6] and it provides a sufficiently accurate representation of the fighter aircraft aerodynamics to be able to evaluate different engine concepts on an aircraft level.

Chapter 2

Aircraft performance and conceptual design

2.1 Aircraft mission and conceptual design

All engine performance analyses conducted were carried out for an aircraft presented in [51]. The aircraft is shown in Figure 2.1 and some of its key characteristics are given in Table 2.1. It was conceptually designed for a mission, illustrated in Figure 2.2, which was first presented in [55] and then more thoroughly described in [51].

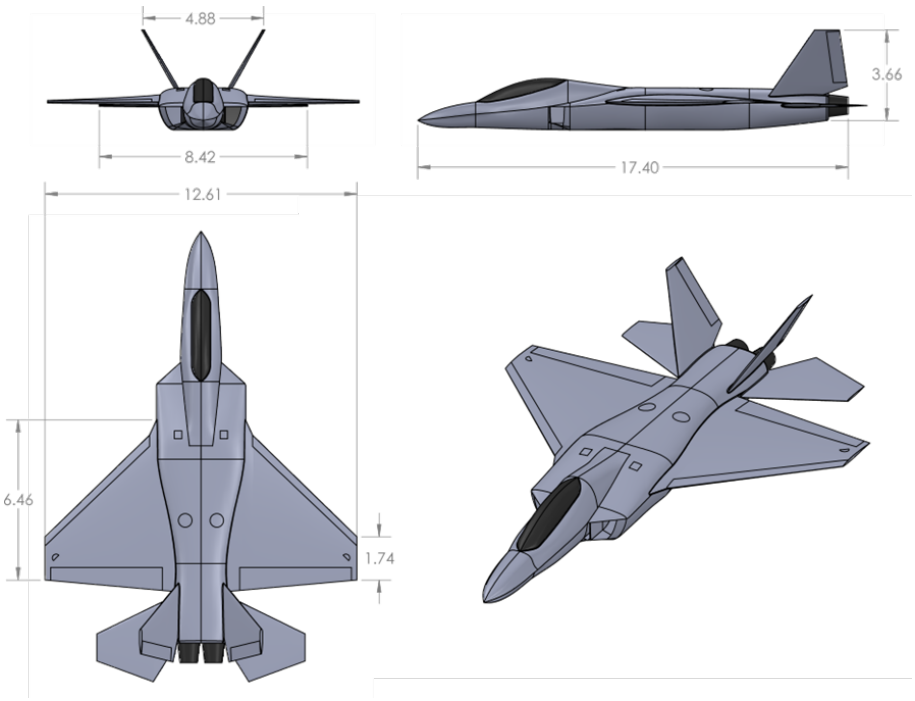

Figure 2.1: The fighter aircraft concept [51].

Table 2.1: Characteristics of the aircraft [51, 56].

Max takeoff mass	m_{TO}	21,920	kg
Empty mass	m_e	12,620	kg
Payload mass	m_p	4,500	kg
Takeoff wing loading	$(W/S)_{TO}$	3,360	N/m^2
Range	R	1,500	nm
Number of engines	n_e	2	

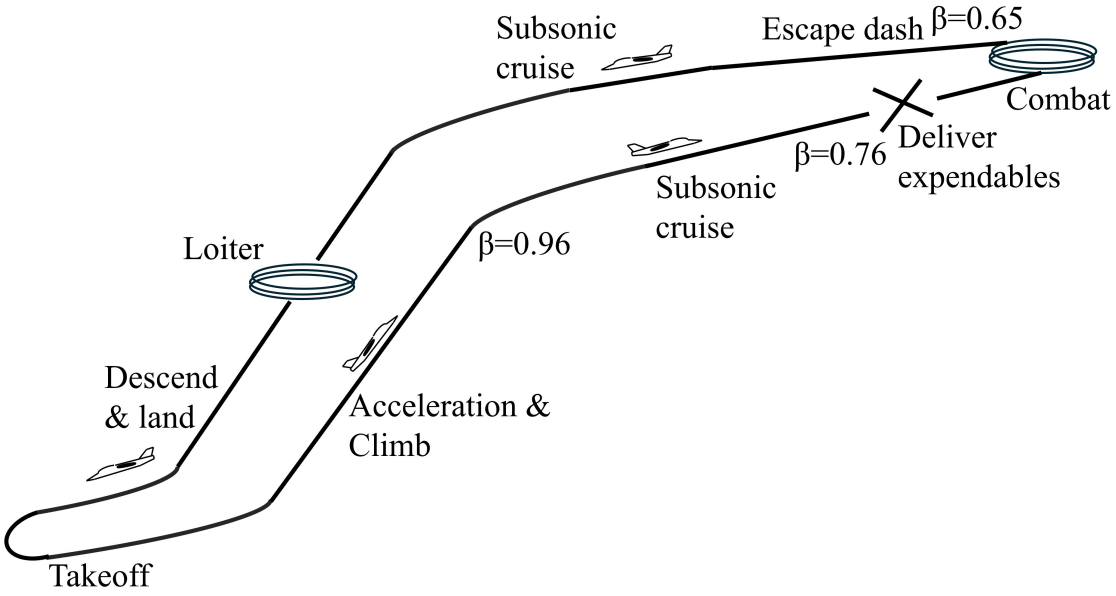

Figure 2.2: The mission profile used for aircraft design [49, 51, 56].

The mission consists of the following phases [56]:

1. Warm-up and takeoff
2. Acceleration and climb
3. Subsonic cruise
4. Payload drop
5. Combat
6. Escape dash
7. Subsonic cruise
8. Fuel reserves
9. Descend to land

Driving factors for aircraft design have included requirements for a high thrust-to-weight ratio (T/W), high weapons load capacity, reduced radar cross section, aircraft robustness, and high supersonic speed capability. These requirements are intended

to provide the aircraft with attributes such as short takeoff distances, high maneuverability, ability to engage a large number of targets, and high survivability [57]. The conceptual design process resulted in a number of initial thrust requirements that are presented in Table 2.2.

Table 2.2: Aircraft thrust requirements [51, 56].

No.	Phase	Description	A/B	Thrust	h	M
1	1	Warm-up	no	132.0 kN	610 m	0.0
2	1	Runway acceleration	yes	221.4 kN	610 m	0.1
3	1	Runway acceleration	yes	225.8 kN	610 m	0.18
4	2	Flight acceleration	yes	254.6 kN	610 m	0.44
5	2	Climb and acceleration	yes	255.6 kN	2743 m	0.775
6	2	Climb and acceleration	yes	157.8 kN	7010 m	0.875
7	3	Subsonic cruise	no	24.8 kN	9144 m	0.9
8	5	Sustained turn	yes	201.2 kN	9144 m	1.6
9	5	Sustained turn	yes	106.4 kN	9144 m	0.9
10	6	Escape dash	yes	227.8 kN	9144 m	2.0

2.2 Aircraft performance and aerodynamics

2.2.1 Aircraft performance modeling

The initial thrust requirements of the aircraft, presented in Table 2.2 were used to size the engine as described in Chapter 3. Once a more detailed engine model has been developed, there is reason to evaluate how the aircraft's capabilities are affected in different parts of the mission. Of even greater interest is being able to evaluate how different engine concepts affect the aircraft's performance. For this reason, an aircraft performance model was developed. Its purpose is to produce realistic thrust requirements for the aircraft for various maneuvers throughout the flight envelope, and it enables interactive aircraft/engine performance studies to be carried out. It has been developed using methods described in [1, 52, 53, 58]

Forces are calculated, applying Newton's second law of motion, using the basic equations (2.1) and (2.2). These equations reflect the forces in the velocity direction of the aircraft and the forces perpendicular to the velocity direction of a wind axis system as illustrated in Figure 2.3.

$$\sum F_x = T\cos\epsilon - D - W\sin\gamma \tag{2.1}$$

$$\sum F_z = T\sin\epsilon + L - W\cos\gamma \tag{2.2}$$

In Figure 2.3, V or V_∞ refers to the true airspeed of the aircraft. Since wind is not taken into account in performance calculations, $V = V_\infty = V_G$ applies [1]. In most flight cases, the thrust inclination angle ϵ, i.e. the inclination of the aircraft relative to the flight direction, is quite small. For such flight cases, the impact of ϵ

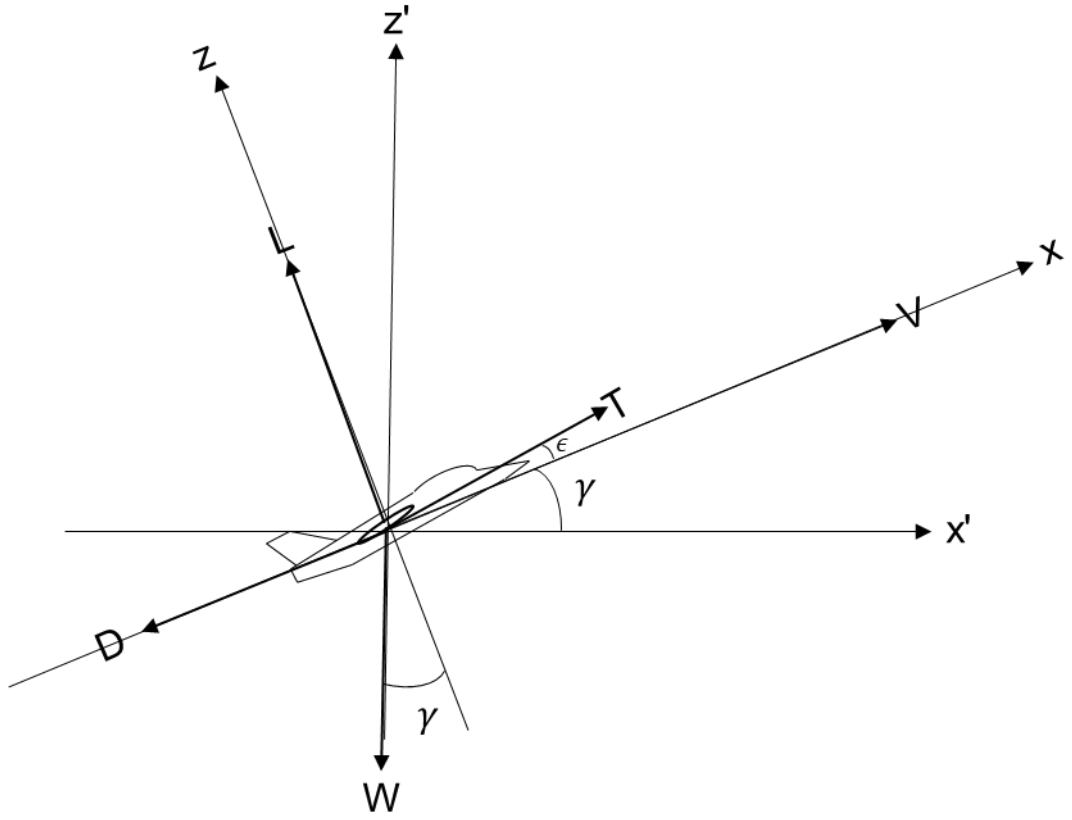

Figure 2.3: The forces acting on the aircraft [56].

can be neglected and $\cos\epsilon \approx 1$ and $\sin\epsilon \approx 0$. In the aircraft performance code, this approximation is used for all flight cases.

To calculate aircraft performance parameters such as acceleration time, turn performance or climb time, specific energy h_e, given by Equation (2.3) and specific excess power P_s, given by Equation (2.4) are used [1, 52]. The most fuel-efficient climb path is calculated using Equation (2.5) [52]. The specific range R_s, and the specific endurance E_s, are given by Equations (2.6) and (2.7) [52]. The thrust specific fuel consumption ($TSFC$) of Equation (2.5), (2.6) and (2.7) is given in Equation (2.8). It is also common to express TSFC as shown in Equation (2.9). An alternative representation of the specific fuel consumption (SFC), representing the fuel consumption relative to the installed net thrust (F_N) is given in Equation (2.10).

$$h_e = h + \frac{V^2}{2g} \tag{2.3}$$

$$P_s = \frac{V(T-D)}{W} = \frac{dh}{dt} + \frac{V}{g}\frac{dV}{dt} \tag{2.4}$$

$$f_s = \frac{dh_e}{dW_f} = \frac{dh_e/dt}{dW_f/dt} = \frac{P_s}{TSFC \times T} \tag{2.5}$$

$$R_s = \frac{dR}{dW} = \frac{V}{-TSFC \times T} \tag{2.6}$$

$$E_s = \frac{dE}{dW} = \frac{V}{-TSFC \times T} \tag{2.7}$$

$$TSFC \equiv \frac{dW_f/dt}{T} \left[\frac{N/s}{N}\right] \tag{2.8}$$

$$TSFC \equiv \frac{dm_f/dt}{T} \left[\frac{kg/s}{N}\right] = \frac{dm_f/dt}{T} \times 10^6 \left[\frac{mg/s}{N}\right] \tag{2.9}$$

$$SFC \equiv \frac{dm_f/dt}{F_N} \left[\frac{kg/s}{N}\right] = \frac{dm_f/dt}{F_N} \times 10^6 \left[\frac{mg/s}{N}\right] \tag{2.10}$$

Equation (2.11) is used to calculate the aircraft drag coefficient [1, 52, 53]. Lift L, and drag D are calculated using Equation (2.12) and (2.13), in which dynamic pressure q is given by Equation (2.14) [1].

$$C_D = C_{D_0} + KC_L^2 \tag{2.11}$$

$$D = qS_{ref}C_D \tag{2.12}$$

$$L = qS_{ref}C_L \tag{2.13}$$

$$q = \frac{1}{2}\rho V^2 \tag{2.14}$$

2.2.2 Parasite drag

Skin friction drag is the main contributor to the subsonic parasite drag of an aerodynamically well-designed aircraft and the ratio of skin friction drag to parasite drag is quite consistent [52]. This makes it possible to estimate the parasite drag, including form and interference drag, of the aircraft using an equivalent skin friction coefficient C_{f_e} [54]. C_{f_e} relates the parasite drag C_{D_0} to the incompressible flat-plate turbulent flow skin friction coefficient and can be estimated from a relatively extensive amount of publicly available information from flight test data for similar aircraft [54]. Equation (2.15) illustrates how the parasite drag coefficient C_{D_0}, can be estimated from C_{f_e}, the wetted area S_{wet}, and the wing reference area S_{ref}.

$$C_{D_0} = C_{f_e}\frac{S_{wet}}{S_{ref}} \tag{2.15}$$

In an attempt to improve the analysis and obtain a better estimate of the changes in Reynold's number that are due to variations in altitude and Mach number, the parasite drag calculation model was refined. The skin friction coefficient of the aircraft was calculated with contributions from the fuselage, wings, tails, and tail

fins using Equation (2.16) which estimates the flat plate skin friction coefficient for turbulent flow [52]. The Reynold's number is provided in Equation (2.17) and the dynamic viscosity is calculated using Sutherland's law for air, see Equation (2.18) [59]. The subsonic cutoff Reynold's number is given by Equation (2.19) and the supersonic cutoff Reynold's number is calculated using Equation (2.20) [52]. The skin friction drag constitutes 60% of the total parasite drag of the fighter aircraft [53]. The described method provides a realistic drag estimate for the fighter aircraft, more accurate than the equivalent skin friction method, although less complicated than the component buildup method, in which the form factors and interference factors of each individual component must be calculated [52, 54].

$$C_f = \frac{0.455}{(\log Re)^{2.58}(1 + 0.144M^2)^{0.65}} \tag{2.16}$$

$$Re = \frac{\rho V l}{\mu} \tag{2.17}$$

$$\mu = 1.71 \times 10^{-5} \left(\frac{T_0}{273.0}\right)^{1.5} \left(\frac{273.0 + 110.4}{T_0 + 110.4}\right) \tag{2.18}$$

$$Re_{cutoff} = 38.21 \left(\frac{l}{k}\right)^{1.053} \tag{2.19}$$

$$Re_{cutoff} = 44.62 \left(\frac{l}{k}\right)^{1.053} M^{1.16} \tag{2.20}$$

Figure 2.4 illustrates how this drag model relates to the values of equivalent skin friction coefficients for typical fighter and bomber aircraft [52, 54]. Figure 2.4 also shows the estimate of parasite drag using the improved method, but with the assumption of a more slender aircraft configuration where two-thirds of the subsonic parasite drag is due to skin friction drag [54].

The parasite drag in supersonic flight is modeled as the sum of skin friction drag and wave drag. Equation (2.21) is used to calculate wave drag [52], where the $(\frac{D}{q})_{Sears-Haack}$ term in Equation (2.21) corresponds to the drag of an ideal Sears-Haack body [60], calculated with Equation (2.22). The leading-edge sweep Λ_{LE} in Equation (2.21) is given in degrees.

$$\left(\frac{D}{q}\right)_{wave} = E_{WD}\left[1 - 0.2(M - 1.2)^{0.57}\left(1 - \frac{\pi \Lambda_{LE}{}^{0.77}}{100}\right)\right]\left(\frac{D}{q}\right)_{Sears-Haack} \tag{2.21}$$

$$\left(\frac{D}{q}\right)_{Sears-Haack} = \frac{9\pi}{2}\left(\frac{A_{max}}{l}\right)^2 \tag{2.22}$$

The parasite drag models for subsonic and supersonic flight are merged within the transonic flight regime with an empirical method described in [52, 54]. The fighter aircraft parasite drag variation with Mach number at an altitude of 9 km is illustrated in Figure 2.5. It can be compared with drag maps of existing fighter aircraft presented in [52, 53].

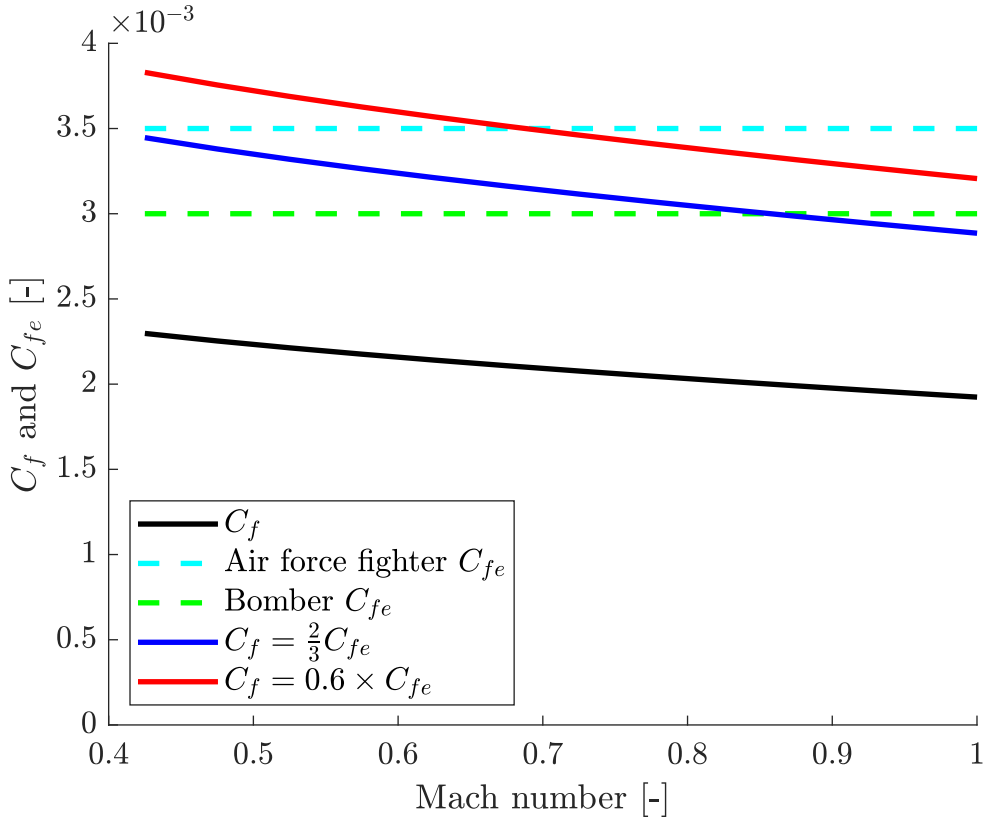

Figure 2.4: C_f and C_{f_e}. Altitude 9 km.

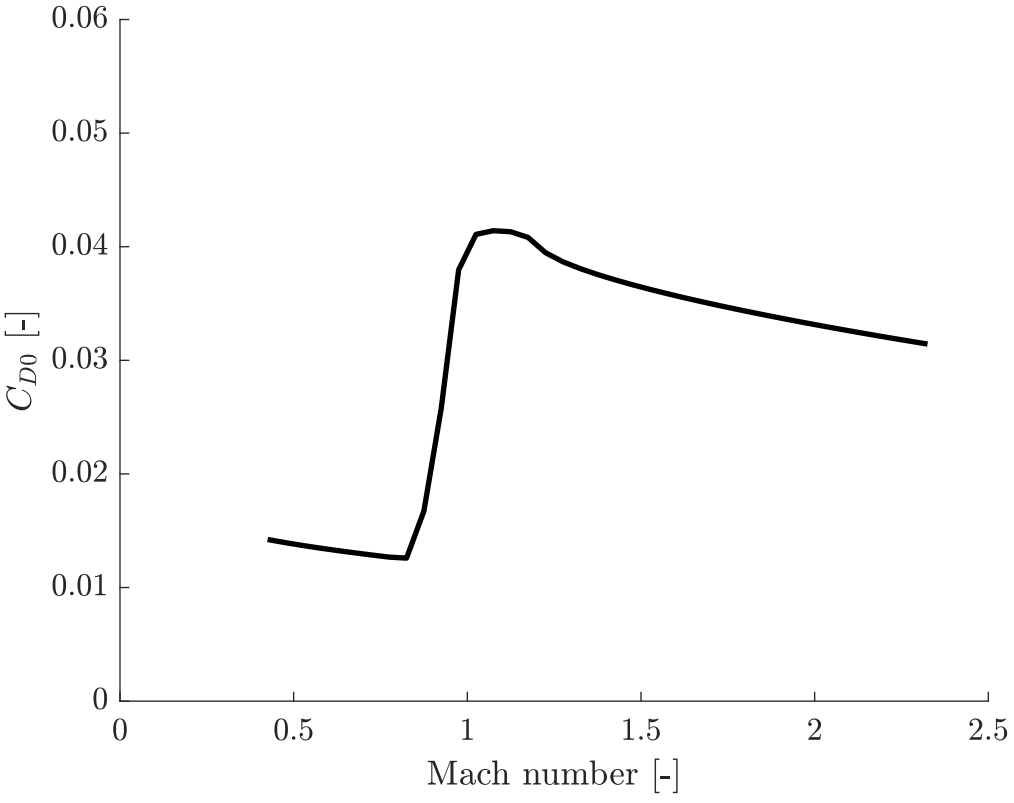

Figure 2.5: Parasite drag of the fighter aircraft. Altitude 9 km.

2.2.3 Lift induced drag

Lift induced drag of the fighter aircraft is estimated, using the leading-edge suction method [52–54, 61, 62], governed by Equations (2.23), (2.24) and (2.25). The slope of the lift curve C_{L_α} in Equation (2.25) is estimated using a method proposed in [52, 63, 64].

$$K = SK_{100} + (1 - S)K_0 \tag{2.23}$$

$$K_{100} = \frac{1}{\pi AR} \tag{2.24}$$

$$K_0 = \frac{1}{C_{L_\alpha}} \tag{2.25}$$

The leading-edge suction parameter S is determined by the design lift coefficient $C_{L_{design}}$, and the lift coefficient C_L in a certain flight maneuver as shown in Equation (2.26). Two values of $C_{L_{design}}$ have been used. A $C_{L_{design}}$ value of 0.18, chosen to optimize the performance of subsonic cruise, was later replaced by a $C_{L_{design}}$ value of 0.5 to achieve improved maneuverability in the more challenging phases of the fighter mission. Both these $C_{L_{design}}$ values and their impact on the leading edge suction parameter, are illustrated in Figure 2.6.

$$S = f(C_L, C_{L_{design}}) \tag{2.26}$$

Leading edge suction is deteriorated with the formation of shocks at the leading edge [52]. For that reason, the modeled leading-edge suction gradually decreases, starting from the drag divergence Mach number. At the Mach number where the leading-edge becomes supersonic and for higher Mach numbers, no leading-edge suction is assumed. An illustration of the calculated K values with $C_{L_{design}} = 0.5$ at altitudes of 9 km and 12 km and an aircraft weight fraction $\beta = 0.96$ is given in Figure 2.7. Typical values for high-performance fighter-type aircraft from [49] with current and expected future technology level are added for comparison.

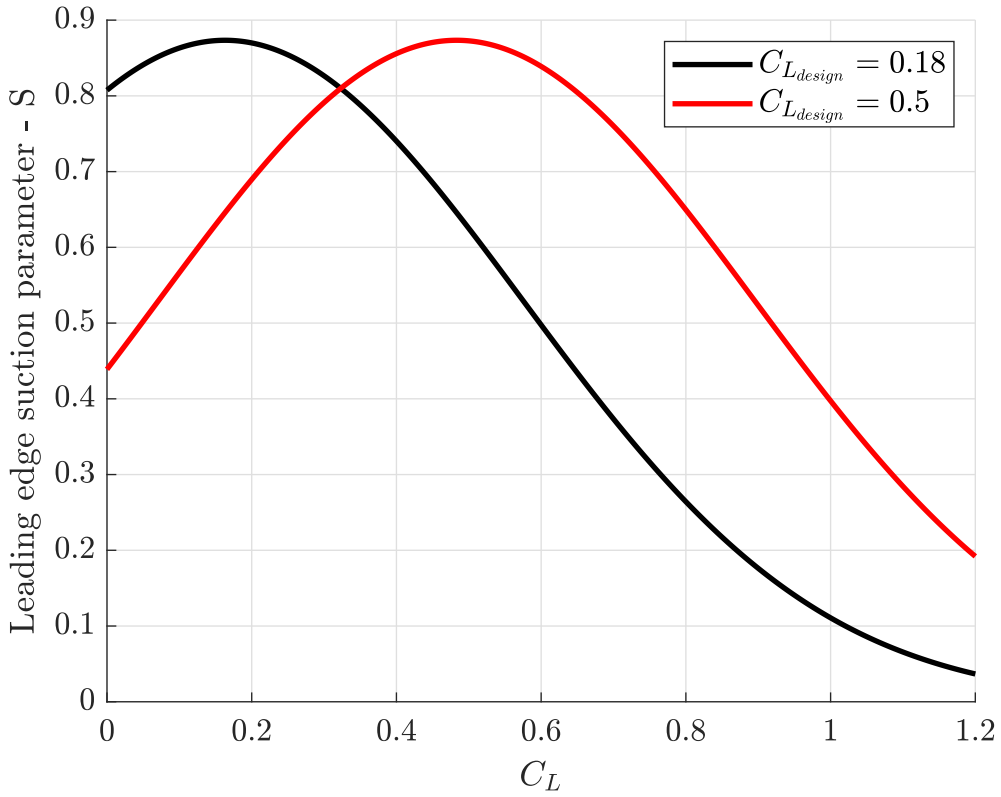

Figure 2.6: Leading-edge suction with $C_{L_{design}} = 0.18$ and $C_{L_{design}} = 0.5$.

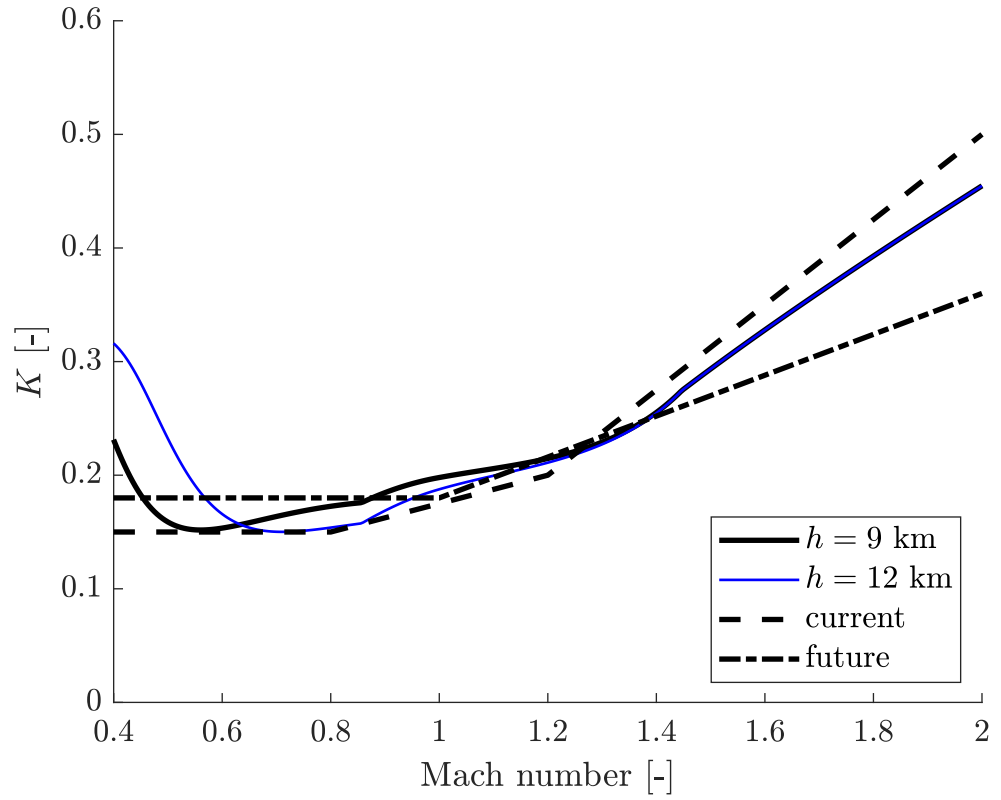

Figure 2.7: K calculated with the leading-edge suction method alongside typical values for fighter-type aircraft with current and future technology [49].

Chapter 3

Engine design

A low-bypass-ratio mixed-flow turbofan engine model was developed to meet the requirements of section 2.1 and Table 2.2. This model has gradually developed over the course of the project. Chapter 3 is divided into three subsections. The engine modeling procedure is described in Section 3.1. When evaluating different engine concepts at the aircraft level, aspects of engine integration and installation effects become increasingly important. This topic is highlighted in Section 3.2. Section 3.3 provides motivation for thermodynamic cycle selections, while Section 3.4 describes the control limits that restrict engine operation. In Section 3.5 modeling of the FLADE turbofan engine is described.

3.1 Engine performance modeling

An advanced tool for engine performance modeling, GESTPAN (general stationary and transient propulsion analysis), has been developed at Chalmers University of Technology [38]. It uses a traditional method with two simulation modes, design and off-design mode. The parameters of the thermodynamic cycle selection, described in more detail in Section 3.3, are specified in the design mode.

The interaction between different modules within the engine must satisfy the requirements of work compatibility, flow compatibility, and rotational speed compatibility [65]. When physical systems modeled with differential equations are subject to such algebraic constraints, differential algebraic equations appear [66]. Semi-explicit differential algebraic equations are one special class of differential algebraic equations. These are ordinary differential equations with constraints [67, 68]. In GESTPAN, a set of equations, generally represented by a system of semi-explicit non-linear differential equations as represented by Equation (3.1), are formed [38, 69]. This type of semi-explicit non-linear algebraic equations are common, not only in the solution of fluid flow equations, but also in applications such as electrical network modeling, mechanical systems with constraints, and vehicle dynamics [70, 71].

$$\begin{aligned} \mathbf{x'} &= f(\mathbf{x}, \mathbf{z}) \\ \mathbf{0} &= g(\mathbf{x}, \mathbf{z}) \end{aligned} \tag{3.1}$$

The x variables of Equation (3.1) are differential variables and the z variables are algebraic variables [69]. For the particular case of steady state, **x'** in Equation (3.1) becomes a zero vector (i.e. $x'_1 = x'_2 = ... = x'_n = 0$). The equation solver of GESTPAN, implemented in Fortran [72], uses a secant method with a Broyden update of the Jacobian [73, 74].

The following modules are implemented in the turbofan engine model:

- Intake
- Fan (LPC)
- Splitter core/bypass flow
- High-pressure compressor (HPC)
- Combustor
- High-pressure turbine (HPT)
- Low-pressure turbine (LPT)
- Unifier (mixer)
- Afterburner (A/B) and nozzle
- Overall supervision unit
- Control selector

The overall supervision unit compiles engine data such as flows, pressure ratios, efficiencies, and thrusts at an overall level while the control selector manages the engine control limits. Additional information on intake implementation is given in Section 3.2. The other modules are described in detail in Appendix A in [38]. Calculating physical gas parameters such as specific heats, specific heat ratios, entropy, and enthalpy is carried out using an open source code presented in [75].

Table 3.1: Engine station numbering.

Station	**Location**
0	Free stream
1	Air intake
2	Fan inlet
3	HPC delivery
4	HPT inlet
5	LPT exit
6	Front face of afterburner
7	Nozzle inlet
8	Nozzle throat
9	Nozzle exit

The turbofan engine is illustrated in Figure 3.1. A schematic engine description, including station numbering according to [76], is provided in Figure 3.1a whereas

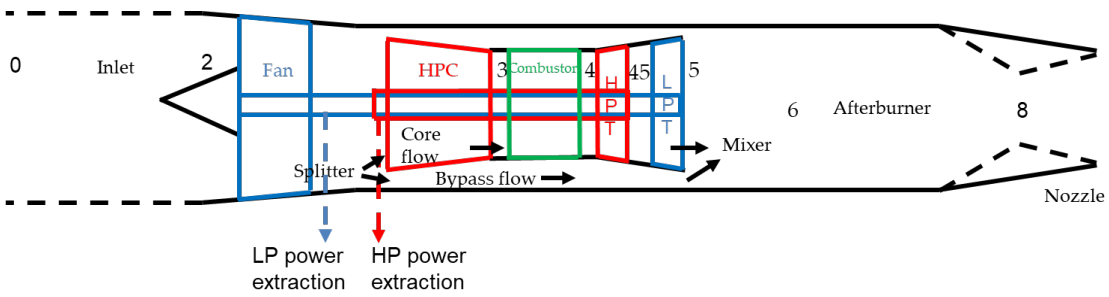

(a) Engine schematic with station numbering [56].

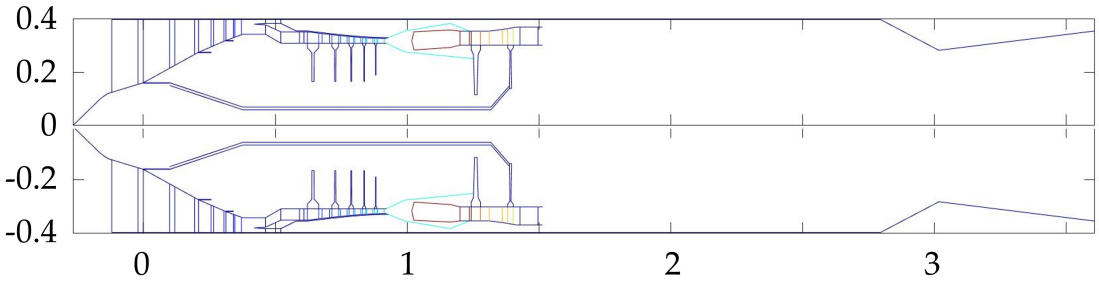

(b) Turbofan engine details based on a figure in [77].

Figure 3.1: Turbofan engine.

a more detailed engine illustration is given in Figure 3.1b. The station numbers of Figure 3.1a are summarized in Table 3.1.

The process of modeling a gas turbine engine involves the selection of the appropriate iteration variables and residuals for Equation (3.1). Table 3.2 summarizes the iteration variables and residuals of the modeled two-spool low-bypass-ratio mixed-flow turbofan engine.

Table 3.2: Iteration variables and residuals of the GESTPAN calculations.

Iteration variables	**Residuals**
Inlet mass flow	Inlet flow compatibility
Fan map β_{fan}	Core flow compatibility
Fan rotational speed	Fan/LPT work compatibility
Core bypass ratio α_{core}	HPC/HPT work compatibility
HPC map β_{HPC}	HPT inlet flow compatibility
HPC rotation speed	LPT inlet flow compatibility
Fuel schedule factor β_f	Static pressure match in unifier
HPT outlet pressure	Afterburner flow compatibility
LPT outlet pressure	Engine control residual

3.2 Aircraft installation effects

The integration of an engine into an aircraft will introduce new drag components and affect its performance in various ways [49]. The intake of a fighter aircraft with the engine installed inside the airframe will induce pressure losses [78]. In flight cases, where the airflow required by the engine is lower than that for which the intake is designed, non-recoverable pre-entry drag will contribute to an increase of aircraft drag compared to operating reference conditions [10, 79–83]. This additional drag is known as spillage drag. Likewise, variations in the exhaust nozzle area and pressure ratio cause changes in the pressure distribution at the aircraft afterbody, which also affect the overall drag of the aircraft [79]. The performance of an integrated engine in an aircraft will also differ from the uninstalled engine performance in the sense that bleed flow, and power will be extracted from the engine for aircraft purposes. Bleed air is typically extracted from one of the later stages of the HPC and is used for aircraft applications such as tank pressurization, environmental control system (ECS), anti-icing systems, aerondynamic compressors, and suction pumps [84]. Power is extracted from either of the two shafts of the aircraft engine, usually the HP shaft, and it is often required for various aircraft systems such as pumps and hydraulic systems, pneumatic systems and control systems [14, 18].

To provide an understanding of how these installation losses relate to the engine's thrust a brief summary of installed engine performance will be presented next. A more thorough description is presented in Appendix E of [49]. The gross thrust F_G of the engine include flow thrust and pressure thrust as shown in Equation (3.2) [38]. The net thrust F_N of the engine is obtained by subtracting the impulse of the free stream airflow that enters the engine from the gross thrust, as illustrated in Equation (3.3). If installed pressure recovery and bleed and power extraction are already accounted for when calculating F_G and F_N, they are referred to as installed gross thrust and installed net thrust [8]. This definition of gross thrust and net thrust is applied here. To calculate the installed thrust of the engine T_e, the spillage drag D_{spill} and the afterbody drag D_{aft} must be subtracted from F_N, as shown in Equation (3.4). The thrust of the aircraft T, used in Equations (2.1) and (2.2), is finally obtained from Equation (3.5) multiplying the thrust of the engine T_e with the number of engines installed in the aircraft n_e.

$$F_G = \dot{m}_9 V_9 + A_9(p_9 - p_\infty) \tag{3.2}$$

$$F_N = F_G - \dot{m}_0 V \tag{3.3}$$

$$T_e = F_N - D_{spill} - D_{aft} \tag{3.4}$$

$$T = n_e T_e \tag{3.5}$$

In the following, a description of how installation losses have been estimated in aircraft/engine performance modeling is presented.

The modeled intake is a fixed normal-shock intake. Its advantages are its lower weight and reduced complexity compared to an intake with variable geometry and that it can nevertheless provide good performance for flight velocities up to approximately 1.6 M [11, 85].

However, the intake is affected by losses that have a significant impact on engine performance. Three important sources of pressure losses are considered. The first is lip losses that occurs due to flow accelerations around the intake lip in flight cases with low aircraft speeds and high engine flow requirements [80]. The second is losses in the intake duct, and the third is shock losses associated with supersonic flight.

An important parameter for estimating both pressure losses and spillage drag is the mass flow ratio (MFR), which relates the engine flow requirements to the stream tube that is captured by the inlet. MFR is given by Equation (3.6), in which the area of the stream tube that enters the engine is represented by A_∞. This area can be determined from Equation (3.7). V_∞ denotes the free-stream velocity, ρ_∞ is the ambient air density, and m_a is the airflow required by the engine.

$$MFR = \frac{A_\infty}{A_c} = \frac{\dot{m}_a}{A_c V_\infty \rho_\infty} \tag{3.6}$$

$$\dot{m}_a = A_\infty V_\infty \rho_\infty \tag{3.7}$$

Lip losses

The intake is matched to the free stream tube of air when $MFR = 1$. For cases where $MFR > 1$, which typically corresponds to a flight case with high air flow requirements at low speed, air must be drawn into the intake from a larger free-stream tube of air [80]. This leads to flow separations and increased losses inside the intake, especially in fighter aircraft, which use sharp lip intakes to reduce supersonic drag [52, 80]. Intake losses are therefore computed as a function of MFR as illustrated by Equation (3.8).

$$\left(\frac{\Delta p}{p_0}\right)_{lip} = f(MFR) \tag{3.8}$$

Duct losses

Duct losses are modeled as a function of corrected mass flow and cross-sectional area of the duct as illustrated in Equation (3.9). Duct losses increase with flow velocities [86] and these flow velocities, in turn, depend on the corrected mass flow and the cross-sectional area of the duct.

$$\left(\frac{\Delta p}{p_0}\right)_{duct} = f\left(\frac{\dot{m}\sqrt{T_0}}{p_0}, A_{duct}\right) \tag{3.9}$$

Supersonic losses

As an aircraft enters the supersonic region of flight, shocks form in front of the intake. p_{01} and p_{02} are the stagnation pressures in front of (1), and behind a normal shock (2), given by Equation (3.10) [14]. With the presence of an external surface such as the aircraft fuselage in front of the intake, it can be expected that the loss of pressure through the shock is somewhat alleviated compared to that of a normal shock described by Equation (3.11) [80]. The shock losses of the normal-shock fixed geometry intake are assumed to constitute 75% of a normal shock ($\alpha_{shock} = 0.75$) given by Equation (3.11).

$$\left(\frac{p_{02}}{p_{01}}\right) = \left(\frac{(\gamma+1)M_1^2}{(\gamma-1)M_1^2+2}\right)^{\frac{\gamma}{\gamma-1}} \left(\frac{\gamma+1}{2\gamma M_1^2-(\gamma-1)}\right)^{\frac{1}{\gamma-1}} \tag{3.10}$$

$$\left(\frac{\Delta p}{p_0}\right)_{supersonic} = \alpha_{shock}\left(1-\frac{p_{02}}{p_{01}}\right) \tag{3.11}$$

Spillage drag

The intake capture area, that is, the cross-sectional area of the intake front face, must be sized to provide the required airflow to the engine in different operating conditions [52]. Hence, at flight conditions with lower airflow requirements from the engine, the excess air in a fixed geometry intake will spill outside the intake and contribute to pre-entry drag as illustrated by Equations (3.12) and (3.13). The estimated pre-entry drag of the fighter aircraft illustrated in Figure 2.1 is presented in Figure 3.2 [77, 80]. For a subsonic intake with rounded lips with a well-faired shape, a large share of this pre-entry drag can be recovered by lip suction [80]. Unfortunately, a supersonic intake with the need for sharp lips [6, 87] does not offer the same advantage [49, 80], even if different intake designs and intake lip thickness distributions may be more or less favorable in terms of lip suction and pre-entry drag cancellation [88]. Spillage drag of the fighter aircraft is estimated by Equation (3.14) applying a method proposed in [8, 81], where $\alpha_{spill} = 0.9$. This α_{spill} represents an intake with sharp lips, designed for good supersonic performance.

$$D_{pre} = (p_c - p_\infty)A_c + \rho_c V_c^2 A_c - \rho_\infty V_\infty^2 A_\infty \tag{3.12}$$

$$C_{D_{pre}} = \frac{D_{pre}}{q_\infty A_c} \tag{3.13}$$

$$D_{spill} = \alpha_{spill} D_{pre} \tag{3.14}$$

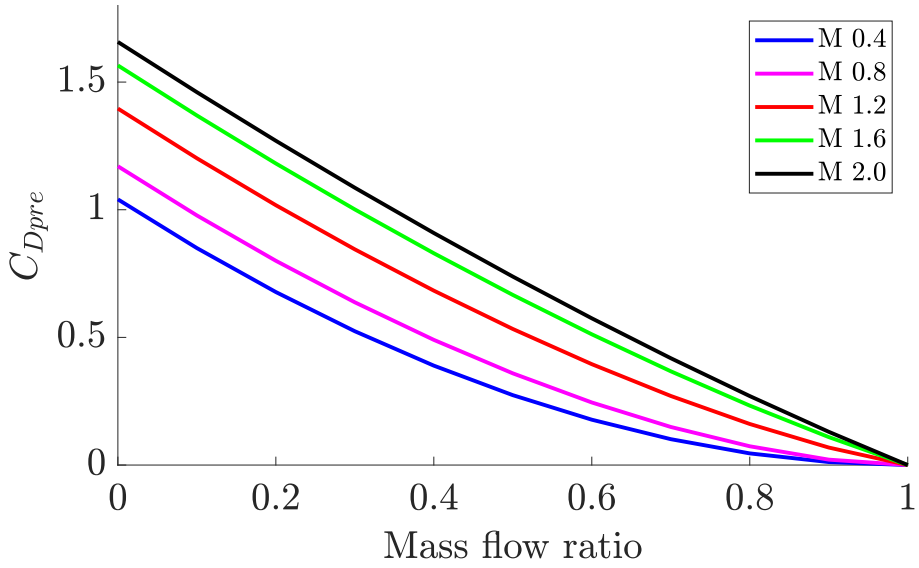

Figure 3.2: Pre-entry drag of the fighter aircraft [77, 80].

Afterbody drag

Separation of boundary layer in the afterbody of an aircraft causes pressure drag, which contributes to the overall drag of the aircraft [49]. In addition, twin-engine installations sometimes suffer from losses due to interference [8]. This afterbody drag contribution for a reference state is already included in the drag profile of the aircraft. Variations in the geometry and exhaust area of a fighter aircraft, with changing flight conditions and engine power levels, will nevertheless cause fluctuations in the external drag of the aircraft [8]. These drag variations are considered installation effects and are taken into account in the afterbody drag calculations. For an aircraft designed for high Mach number operation, the afterbody drag may be significant [7, 8]. However, afterbody drag was neglected. The exact shape of the afterbody is rarely decided in the conceptual design phase [49] and in the comparative studies that have been conducted, the variations in the nozzle exit area between compared cases were small if any. Although the reduction of afterbody drag is one of the motivations for VCEs [7, 89, 90], the potential for afterbody drag reductions with the FLADE turbofan engine, further described in Section 3.5, is considered minor for the evaluated fighter aircraft. A study carried out in [39] for an engine with greater flexibility in flow variation indicated a half-percent reduction in aircraft drag for subsonic flight and supersonic flight with military power (maximum dry power, maximum power without afterburning).

Shaft power extraction

The conditions for extracting power vary depending on the flight case. Mechanical power off-take, whether for electrical or hydraulic purposes, has a much greater impact on engine performance at higher altitudes and lower speeds, where absolute power off-take constitutes a greater share of total power produced by the turbine concerned [15]. To better illustrate this, a corrected measure of power off-take can be

used [49]. Equation (3.15) shows how the corrected power extraction, P_{cTO}, relates to the absolute power extracted, P_{TO}, when normalized to standard sea-level conditions. Figure 3.3 illustrates the variation of P_{cTO} over the flight envelope with an absolute power off-take $P_{TO} = 100$ kW when the engine operates at military power. Figure 3.3 shows that for a constant power off-take ($P_{TO} = 100$ kW) the corrected power off-take is tripled ($P_{cTO} = 300$ kW) at an altitude of 11 km and a flight Mach number of 0.8 compared to the sea level static case ($P_{cTO} = 100$ kW).

$$\frac{P_{cTO}}{P_{TO}} = \frac{\dot{m}_{0,std} h_{0,std}}{\dot{m}_0 h_0} \tag{3.15}$$

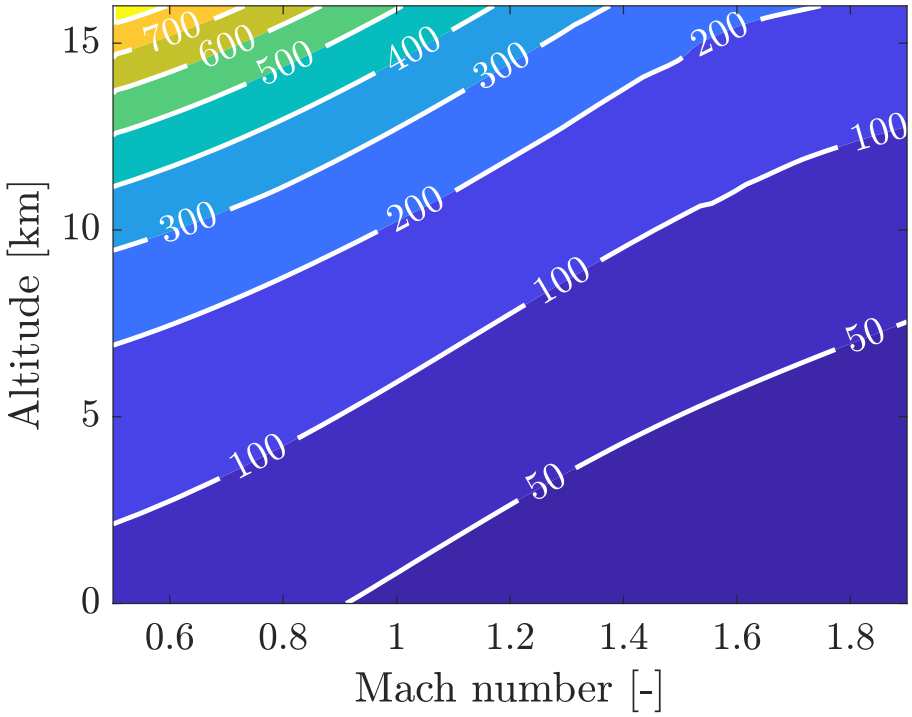

Figure 3.3: Corrected power off-take with an absolute off-take of 100 kW.

For the study of large power extraction, a total absolute power extraction of 1.8 MW was assumed from the two engines in the different operating points. From Equation (3.15) and Figure 3.3, it can be concluded that such a large power off-take should have the greatest impact on the subsonic cruise phase, that is, thrust requirement number 7 in Table 2.2. This is a part-power requirement at subsonic speed and relatively high altitude, where the engine operates with reduced airflow compared to the military power case.

Four cases were compared. In addition to the baseline case without power extraction, 900 kW per engine was extracted solely from the HP shaft, solely from the LP shaft, or as a combined power extraction with 450 kW from each shaft [51, 55, 56]. For the FLADE turbofan engine study, an absolute HP power extraction of 150 kW per engine was assumed [6, 49, 77, 91] in all operating points.

Bleed flow extraction

When referring to bleed flow as part of engine installation effects, this is the bleed flow used for aircraft systems. This bleed flow should not be confused with the internal cooling flow of the engine, sometimes also referred to as bleed flow [14, 49]. This cooling flow will be handled in Section 3.3 The modeled bleed flow is extracted from the last stage of the HPC [92]. In the study of large power extraction, no bleed air was extracted, while 1 kg/s bleed flow was simulated for off-design cases in the FLADE turbofan engine study [92].

3.3 Engine sizing and design point selection

The purpose of the process for selecting the thermodynamic design was two-fold. First, and most importantly, was the object of determining the thermodynamic cycle of a typical fighter engine. To make the analysis of different engine concepts or different types of operating cases general, typical values for a fighter aircraft engine have been selected. There are now plenty of sources to conduct such a survey, both from literature [15, 49, 85, 93–96] and from data sheets provided by the engine manufacturers. The selection of specific cycle parameters such as core bypass ratio or throttle ratio (TR) will, of course, always depend on strategic considerations, and the design mission of the aircraft [29, 49], but certain characteristics, such as high thrust-to-weight ratio or high specific thrust [3, 27, 28], are after all common to most fighter aircraft.

The thermodynamic cycle parameters of the design point of the engine have always been selected for sea-level static (SLS) conditions, since this is the most openly well-documented condition, both in the literature and from the industry. Other requirements have been evaluated through off-design simulations with constraints. The cycle parameters and the off-design constraints were chosen, with regard to previous experience in the field, but also with expectations of future technological improvements in terms of material and component capability. Such improvements have historically enabled higher operating temperatures, improved efficiency, and higher stage loadings of components, allowing a more compact design [93, 97].

After this initial phase of cycle evaluation, an iterative procedure was followed in which the engine cycle was matched to meet the mission requirements presented in Table 2.2. This included all the parameters involved in the selection of the design point. An example is provided in Figure 3.4, demonstrating the search for a suitable design π_c to meet the thrust requirement for one of the takeoff requirements, point number 2 in Table 2.2, with and without power extraction. The survey was carried out with a common design point core bypass ratio of 0.4 and design point turbine inlet temperature T_4 of 2025 K. Figure 3.4 shows that for a design π_c around 20-30 for the reference case and 25-35 for the power extraction case, the required T_4 to meet the thrust requirement of point 2 is lower.

However, it soon became evident that the tenth requirement, the escape dash, would have a major impact on the cycle design and the selected throttle ratio (TR) of the engine (described in more detail in Section 3.4). This challenging requirement

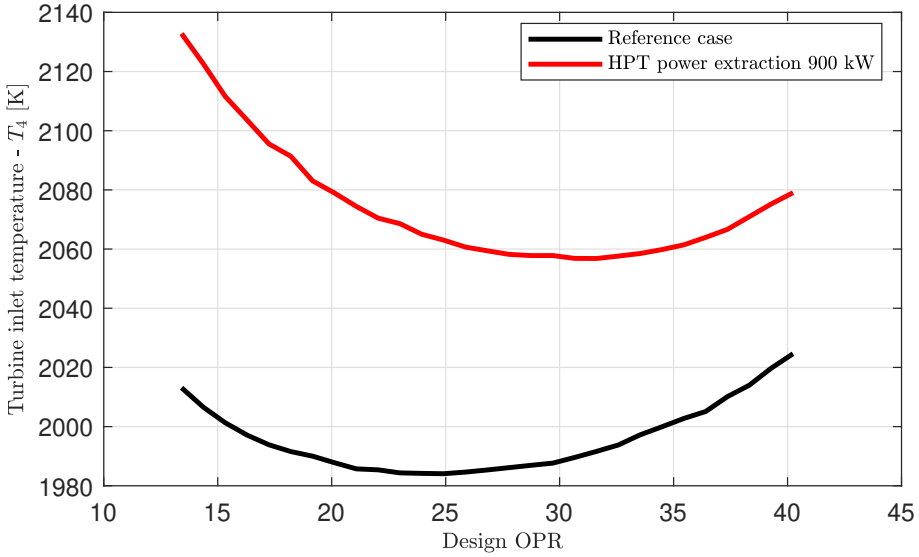

Figure 3.4: Required T_4 for different design π_c, point 2 of the mission thrust requirement, from [55].

largely governed the first cycle design (DP1), illustrated in Table 3.3. At a later stage, this requirement was slightly relaxed to achieve a somewhat more balanced design for the FLADE tubofan engine study (DP2). The key parameters for that design point, chosen for a part-power condition, are also provided in Table 3.3.

Table 3.3: Design point characteristics [56, 77].

Parameter	**DP1**	**DP2**
Altitude	0 m	0 m
Mach number	0.0	0.0
Fan pressure ratio	5.4	3.8
HPC pressure ratio	5.2	6.5
Inlet mass flow	90 kg/s	82 kg/s
Cooling flow fraction	0.2	0.2
Core bypass ratio	0.5	0.5
Turbine inlet gas temperature	2000 K	1650 K
Fan polytropic efficiency	0.89	0.89
HPC polytropic efficiency	0.905	0.905
HPT polytropic efficiency	0.905	0.905
LPT polytropic efficiency	0.91	0.91
Bleed flow	0 kg/s	1.0 kg/s
LPT power extraction	0 kW	0 kW
HPT power extraction	0 kW	0 kW

A high fan pressure ratio was desired to achieve a high specific thrust of the engine [14, 28, 98]. For a military aircraft, a high specific thrust allows the engine to meet challenging thrust requirements with a limited amount of airflow. When the engine can be designed for this lower airflow, the cross-sectional area of the intake

and engine can be kept down. A low cross-sectional area limits the increase in drag of the aircraft in supersonic flight and is very advantageous for a fighter aircraft, designed for supersonic operation [3, 27–29]. However, there are limits to the fan pressure ratio. The introduction of a fourth stage is not attractive as it contributes to an increase in weight and volume of the engine, and the maximum stage loading with current technology limits the fan pressure ratio of a modern three-stage military fan to approximately 5 [3]. Therefore, an FPR of 5.4, as chosen for DP1 in Table 3.3, is challenging. Nevertheless, over the past fifty years, there has been a steady increase in the pressure ratio per stage in military fan designs [93] and axial flow compressors of today have pressure ratios of approximately 1.7–1.8 [99].

A core bypass ratio of 0.5, as chosen for both DP1 and DP2, is in good agreement with what has been reported in the open literature for military engines [14, 15, 29, 49, 93, 96]. 20% of the core flow is used for cooling, a typical amount of cooling for high technology aero engines [100].

3.4 Engine constraints and limitations

Two of the most important parameters constrain the operation of the engine, applying a method proposed in [49]. At both military power and maximum augmented power (maximum power with afterburning), fuel flow is constrained by π_c under conditions of low flight velocity and high altitude. Figure 3.5 shows the variation of π_c with nondimensional free-stream temperature θ_0. The turbine inlet temperature increases with increasing flight velocities until it reaches its T_4 limit, after which the engine switches to the T_4 limitation as illustrated by Figure 3.5.

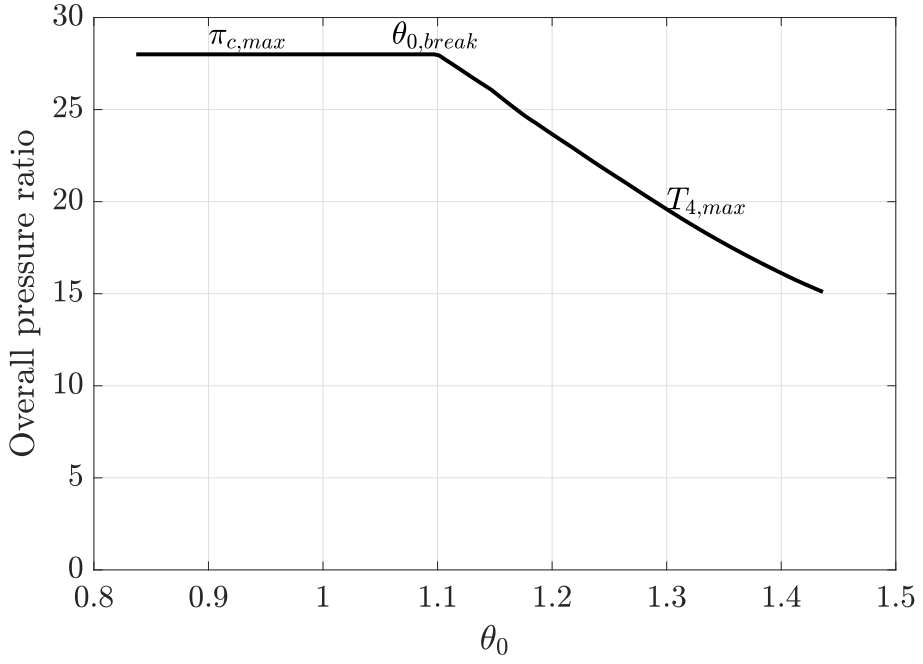

Figure 3.5: Overall pressure ratio variation with non-dimensional stagnation temperature [56] using a method for engine control proposed in [49, 50, 101].

The point where the engine switches from the π_c limitation to the T_4 limitation is called the $\theta_{0,break}$ or the throttle ratio (TR). The TR is a design choice that has a significant impact on the performance of the fighter engine in different parts of the flight envelope. θ_0 and TR are provided in Equations (3.16) and (3.17) [49], where $T_{4,std}$ represents T_4 at military or maximum augmented power and standard sea level static conditions, where engine power is limited by $\pi_{c,max}$.

$$\theta_0 = \frac{T_0}{T_{std}} \tag{3.16}$$

$$TR = \frac{T_{4,max}}{T_{4,std}} = \theta_{0,break} \tag{3.17}$$

Figure 3.6 gives an overview of the control modes in the flight envelope at military power. Figure 3.6a illustrates the distribution of the maximum π_c and the maximum T_4 operations with a TR of 1.06. Although the applied control principle is a highly appropriate method to describe the control principles of a typical combat aircraft engine, the engine power may also be restricted by other limitations, such as maximum N_1, maximum T_3, or maximum P_3 [7, 15, 50, 102]. To aid understanding of how such limitations can affect engine control, Figure 3.6b illustrates where they may become active in the flight envelope.

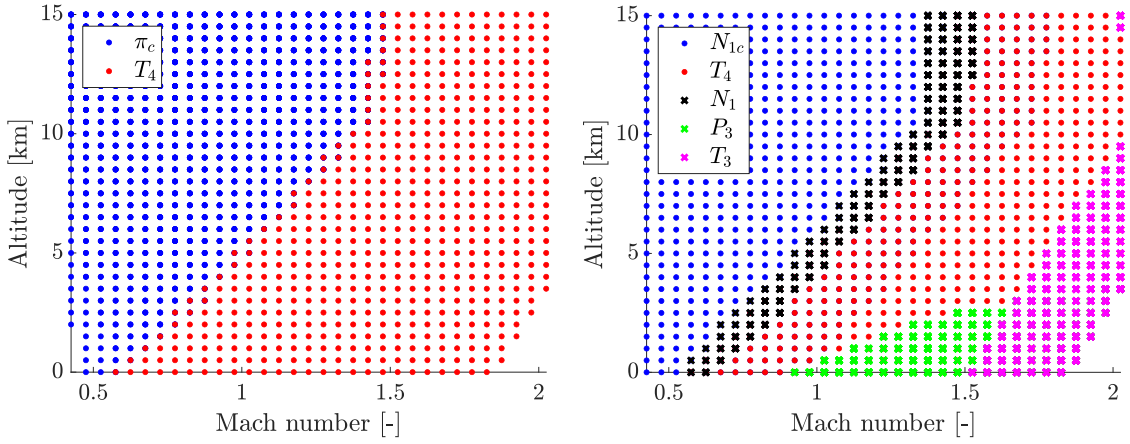

(a) Control schedule for a turbofan engine with $TR = 1.06$ [49, 77].

(b) Typical control limiters of a fighter engine [15, 50].

Figure 3.6: Engine control principles.

If the maximum HP shaft speed N_2 should limit the maximum power operation of the engine, the flight envelope of Figure 3.6b would typically be further restricted in the right parts of the flight envelope currently limited by T_4 [15]. In practical engine control, the corrected fan speed N_{1c}, given in Equation (3.18), is used instead of π_c. Hence, the maximum limit π_c is replaced by a maximum limit N_{1c} in Figure 3.6b. However, T_4 is included in both Figures 3.6a and 3.6b, although in practice it needs to be replaced by another temperature measurement such as T_{45} due to the high turbine inlet temperature [15].

$$N_{1c} = \frac{N_1}{\sqrt{\frac{T_{02}}{T_{std}}}} \tag{3.18}$$

The constraints of the two engines, presented in Table 3.3, are provided in Table 3.4. A maximum turbine inlet temperature of 2260 K for the F135, reported in [103] was chosen for DP1. This extremely high T_4, in combination with a high specific thrust cycle selection (see Table 3.3) and a maximum π_c of 28 was required to meet all thrust requirements in Table 2.2. Turbine inlet temperatures of this magnitude are very challenging with respect to material strengths, thermal corrosion, lifetime of hot parts and cooling requirements [102–104]. As the conceptual design process progressed and the escape dash thrust requirement (No. 10) was relaxed, a maximum T_4 of 2075 K as suggested in [91] was selected in conjunction with a limitation π_c of 36. This appears to be a well-balanced choice, although challenging in terms of stage loadings of the HPC and the HPT, and in terms of maximum temperatures at the HPC outlet T_3 [91]. With the expected improvements in turbomachinery, following previous trends in development [93], and the higher temperature capability of the materials used at compressor discharge in future installations [97, 105], this seems realistic.

Table 3.4: Off design point constraints [56, 77].

Parameter	**DP1**	**DP2**
$\pi_{c,max}$	28	36
$T_{4,max}$	2260 K	2075 K

3.5 FLADE turbofan engine

Combat aircraft are traditionally powered by low-bypass-ratio mixed-flow turbofan engines of the type described in the previous sections of Chapter 3. These engines have developed tremendously since they replaced turbojet engines in military aircraft, a little more than half a century ago. The engine thrust-to-weight ratios have increased considerably [3] and the same trend is seen with respect to the specific core power [97]. Although the aircraft's capabilities have improved thanks to these high specific thrust engines, the drawback of poor subsonic performance due to low propulsive efficiency and high installation losses remains. The development of variable cycle engines is an attempt to combine the high specific thrust of a turbojet engine or low-bypass-ratio turbofan engine with improved propulsive efficiencies and reduced installation losses, both in subsonic and supersonic flight [38].

The FLADE is an extension of the fan blades to form an additional compressor on top of the fan that allows an additional bypass flow to be established outside, circumscribing the conventional fan flow [9, 106–108]. In this way, it helps maintain a higher flow in operating cases where the engine would otherwise be throttled down. Such operating conditions occur in part-power flight cases such as in subsonic cruise and loiter, but also in supersonic operation, when the engine is throttled down to not

exceed one of its limiters, as described in Section 3.4. The additional flow maintained by the FLADE under such operating conditions both improves propulsive efficiency and reduces engine spillage drag [107].

The benefits of an external bypass flow are not limited to performance improvements. The increasing heat loads in modern combat aircraft is becoming more and more of a problem [16, 109]. In fact, the flight endurance of a combat aircraft may be limited by insufficient cooling of vital equipment in the aircraft, rather than fuel shortage [110]. An additional bypass flow may be used to cool aircraft systems [16, 37, 111] or to actively cool the engine core [44], thus contributing to a solution to the thermal management problem. In addition, the external bypass flow could potentially be used to reduce the infrared (IR) signature of the nozzle [107] or to suppress engine noise at takeoff [112, 113].

The FLADE has been considered for advanced VCE concepts such as the adaptive cycle engine (ACE) [114–116], but also as a means of improving the flexibility of a conventional turbofan engine. The latter concept, illustrated in Figure 3.7, has been the main focus of this work.

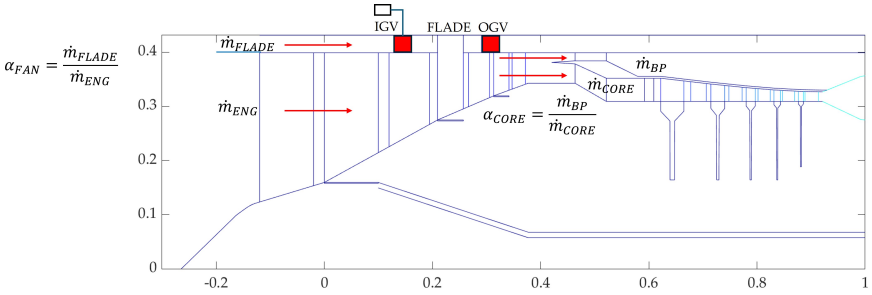

Figure 3.7: Integration of the FLADE component [77].

In addition to the modules presented for the turbofan engine in Section 3.1, the FLADE turbofan engine also includes the following modules:

- VCE mode selector
- Splitter FLADE/turbofan engine flow
- FLADE
- FLADE duct
- FLADE nozzle
- Modules for torque and power transfer

The VCE mode selector can be used to switch between turbofan and FLADE turbofan operation, and is prepared for switching between operating modes of a more complex future VCE model. The modules for torque and power transfer are used to balance the torque and power produced by the LPT with the total torque/power consumed by the fan and the FLADE. More information on FLADE modeling is provided in [42].

Table 3.5: Additional and modified iteration variables and residuals.

Iteration variables	**Residuals**
Fan rotational speed	Fan/FLADE/LPT work compatibility
Fan bypass ratio α_{fan}	FLADE nozzle flow compatibility
FLADE map β_{FLADE}	FLADE/splitter mass flow compatibility

Additional and modified iteration variables and residuals of the FLADE turbofan engine compared to those highlighted in Table 3.2 are presented in Table 3.5.

Inlet guide vanes (IGVs) allow for flow changes for a constant fan speed [117]. IGVs are implemented, using a method proposed in [118] to modulate the flow to the FLADE duct and to limit the relative Mach number in the FLADE by creating a pre-swirl [119, 120]. To allow flow modulation in various parts of the combat aircraft operating envelope with different power levels of the engine, a combined IGV and nozzle schedule was developed. Figure 3.8 illustrates the part-power schedule in subsonic flight. This combined IGV/nozzle control allows FLADE flow reductions to 13% of total airflow [77]. The required minimum flow of the third stream is not available for the turbofan engine and therefore has a considerable impact on the maximum performance of the engine. In previous VCE evaluations, the assumed amount of flow varies. For example, 15% is assumed in [39, 121] to meet the minimum requirements of thermal management, while [36] assumes a more or less complete shut-off of the flow. According to [106], a small flow may be required to reduce air resistance losses and internal local heating in the FLADE duct. In Section 4.2, both the minimum flow alternative and the complete shut-off alternative are considered when evaluating the maximum performance of the engine.

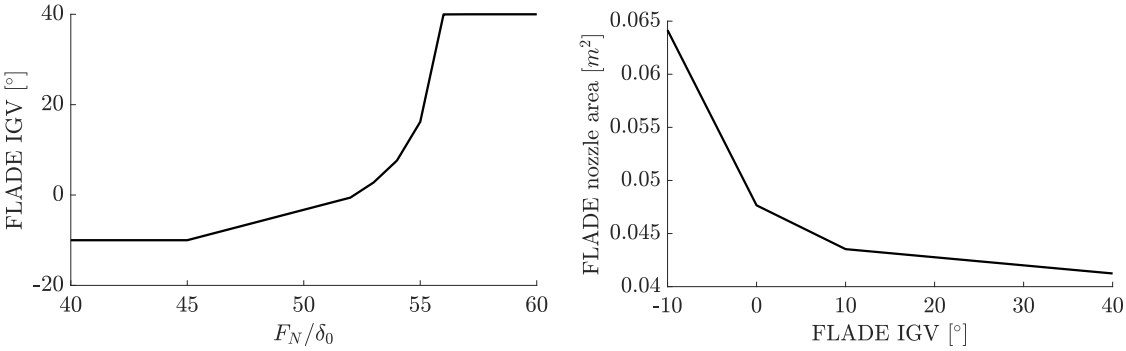

(a) IGV control. (b) Nozzle control.

Figure 3.8: Combined IGV and nozzle control [77].

Different variable cycle concepts may seem more appealing than they actually are. Large flow variations may introduce losses of efficiency in different engine components and flow losses in bypass ducts [7]. For the FLADE turbofan engine, flow losses in the FLADE duct may cancel some of the performance improvements achieved with the concept. The losses of the FLADE duct were calculated using Equations (3.19), (3.20), and (3.21) [86] for three different duct areas, corresponding to 15%, 20%, and 40% of the fan annulus area, where 20% was chosen as a reference area. Losses can

be reduced with a wider duct, as illustrated in Figure 3.9, but at the expense of an increase in the cross-sectional area of the engine. The supersonic drag penalty from this increase in cross-sectional area is taken into account as an increase in A_{max} in Equations (2.21) and (2.22). The calculated losses presented in Figure 3.9 can be compared with the variation of losses with the Mach number in a bypass duct of an engine test reported in [89].

$$-\rho_1 u_1^2 A + \rho_2 u_2^2 A = p_1 A - p_2 A - \int_0^L \pi(D_1 + D_2)\tau_w dx \tag{3.19}$$

$$A = \pi \frac{D_2^2 - D_1^2}{4} \tag{3.20}$$

$$\tau_w = \frac{1}{2}\rho u^2 f \tag{3.21}$$

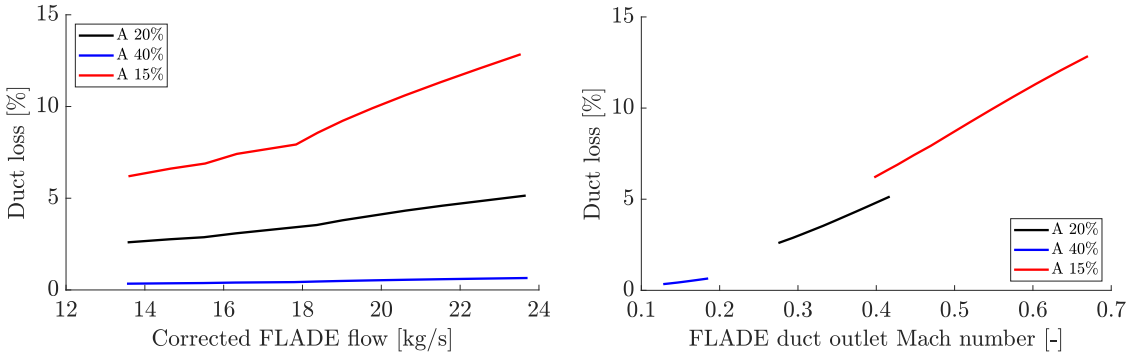

(a) Variation of duct loss with duct area and duct flow.

(b) Variation of duct loss with duct area and Mach number.

Figure 3.9: Losses of the FLADE duct [77].

3.6 Weight estimation

A disadvantage of VCEs is that they involve a high number of additional variable geometry, making them heavier than a corresponding turbofan engine. Many promising concepts, which reduce SFC, have ultimately resulted in increased fuel consumption at an aircraft level due to the increased engine weight [7]. Consequently, to compare two different concepts, the engine weight must be taken into account. A Chalmers developed tool named WEICO (weight and cost estimate), developed for engine conceptual design and sizing [122], was used to estimate weight of the turbofan and the FLADE turbofan engine. These weight estimates were then evaluated using methods reported in [123]. Engine performance data, generated by GESTPAN, is processed by WEICO to produce weight and geometric characteristics of the engine components [124]. Additional weights associated with the FLADE turbofan engine is summarized in Table 3.6.

Table 3.6: Additional weight of the FLADE turbofan engine.

Component	**Δ Weight**
FLADE components	16 kg
Bypass duct	44 kg
Accessories	23 kg
Total	83 kg

Chapter 4

Simulation results

In this chapter, key results are summarized. Chapter 4 is divided into two main parts, covered in Sections 4.1 and 4.2. The first part, based on the analyses presented in [51, 55, 56], focuses on a conventional low-bypass-ratio turbofan engine and large power extraction. In the second part, a performance evaluation of the FLADE turbofan engine is presented.

4.1 Power extraction evaluation

The objective of the first part of the project was to investigate how large power extraction limits the performance of a conventional two-spool low-bypass-ratio mixed-flow turbofan engine. A total of 900 kW was extracted from each engine in all operating points evaluated. Since there are two different options for extracting power from this type of engine, namely, the LP shaft or the HP shaft, both options were evaluated. Consequently, two main cases were prepared in which all power (900 kW) was extracted from either the HP shaft (illustrated with red colour in the figures below) or the LP shaft (blue colour). In addition to these two extremes, a third option would be to distribute the power extraction between the two shafts. This case was also evaluated with power extraction evenly distributed between the two shafts (450 kW from each shaft, illustrated with magenta). The different options were evaluated against the mission requirements specified in Table 2.2 in Section 2.1. These requirements are repeated in Table 4.1 as thrust per engine requirements.

Table 4.1: Engine thrust requirements [51, 56].

No.	Phase	Description	A/B	Thrust	h	M
1	1	Warm-up	no	66.0 kN	610 m	0.0
2	1	Runway acceleration	yes	110.7 kN	610 m	0.1
3	1	Runway acceleration	yes	112.9 kN	610 m	0.18
4	2	Flight acceleration	yes	127.3 kN	610 m	0.44
5	2	Climb and acceleration	yes	127.8 kN	2743 m	0.775
6	2	Climb and acceleration	yes	78.9 kN	7010 m	0.875
7	3	Subsonic cruise	no	12.4 kN	9144 m	0.9
8	5	Sustained turn	yes	100.6 kN	9144 m	1.6
9	5	Sustained turn	yes	53.2 kN	9144 m	0.9
10	6	Escape dash	yes	113.9 kN	9144 m	2.0

The installed thrust of each case can be compared with the reference case without power extraction (black) and the thrust requirements (green) in Figure 4.1. The combined thermodynamic design point DP1 of Section 3.3 and the constraints imposed as described in Section 3.4 allow the engine to meet the thrust requirements of Table 4.1 in the reference case. When a large amount of power is extracted, the engine cannot meet the most stringent requirements of Table 4.1. For this mission, it happens to be the fifth and the tenth requirements. In the combined climb and acceleration phase of requirement five, the engine operates at maximum π_c and cannot meet the required thrust when power is extracted from the LP shaft, as illustrated in Figure 4.1. In the escape dash, requirement number ten, the situation is quite different. This is a high speed point where the engine is operating at its limit T_4, see Figure 4.2. Figure 4.1 shows that the tenth thrust requirement is not met by any of the power extraction alternatives and that the HP power extraction alternative suffers from the worst thrust drop compared to the reference case.

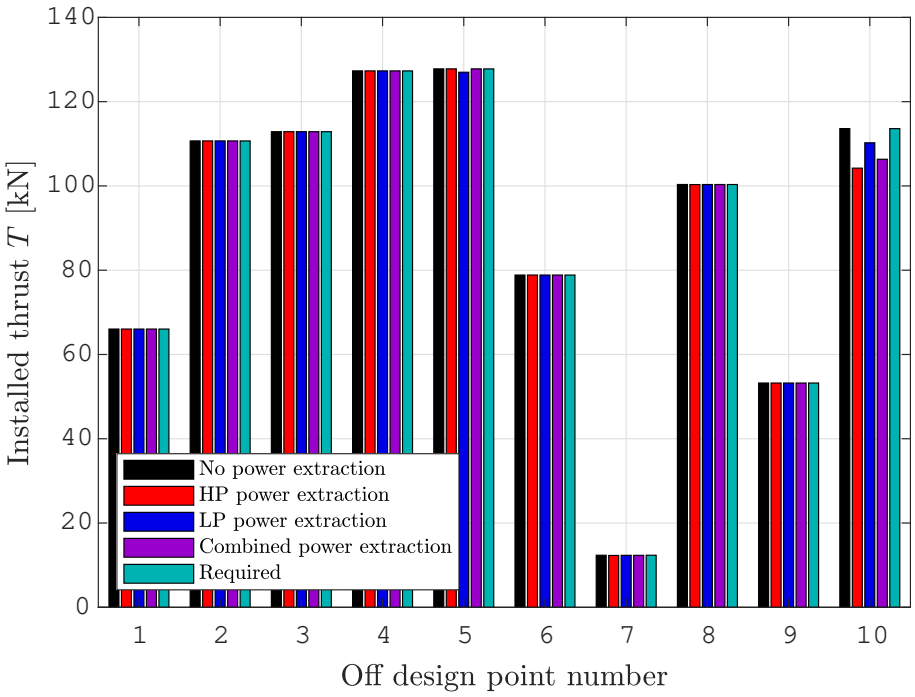

Figure 4.1: Installed thrust and thrust requirement [56].

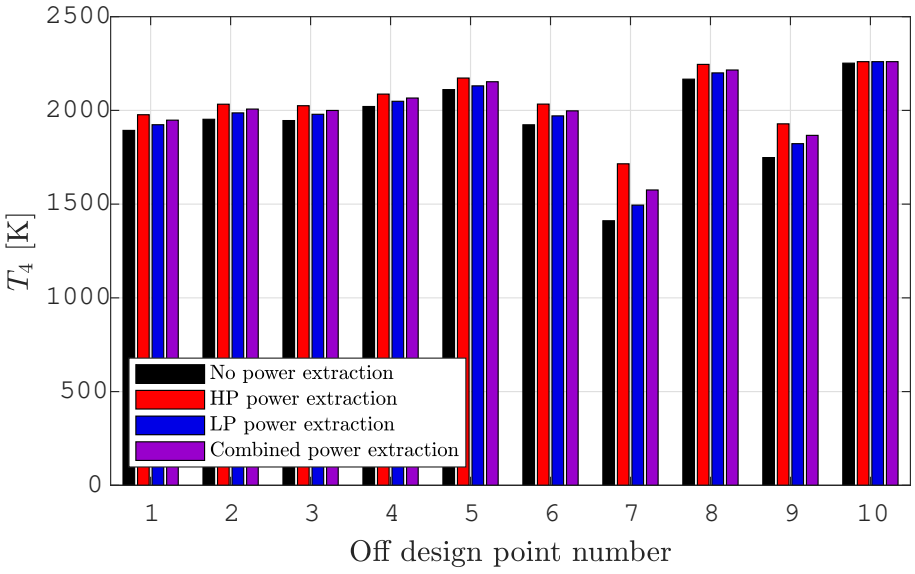

Figure 4.2: Turbine inlet gas temperature [56].

Figure 4.2 shows that HP shaft power extraction leads to the largest increase in T_4 for all requirements 1–9. Since point ten is already operating at or close to maximum T_4 for the reference case, the HP shaft power extraction alternative, which requires the highest temperature increase, is the most constraining. The higher T_4 resulting from the HP shaft power extraction case increases the specific thrust of the engine as long as it is not limited by $T_{4,max}$, but the higher specific thrust is also accompanied by a higher engine TSFC for non-augmented cases. This relative increase in TSFC is illustrated for the non-augmented operating cases warm-up and cruise, represented by points 1 and 7 in Figure 4.3. In contrast to the non-augmented operating cases, an increase in T_4 and specific thrust of the core engine is beneficial for the augmented cases, point 2–6, 8 and 10. Provided that an increase in T_4 of the core engine is acceptable, a slight reduction in TSFC can be achieved for the augmented cases due to the higher efficiency of the core engine compared to afterburning [55]. The addition of heat at the higher pressure of the core engine cycle is always more efficient than burning fuel at the lower pressure in the afterburner [15]. The redistribution of power from the afterburner to the core engine with the higher T_4 of the HP shaft power extraction case is illustrated in the schematic T-S diagram in Figure 4.4.

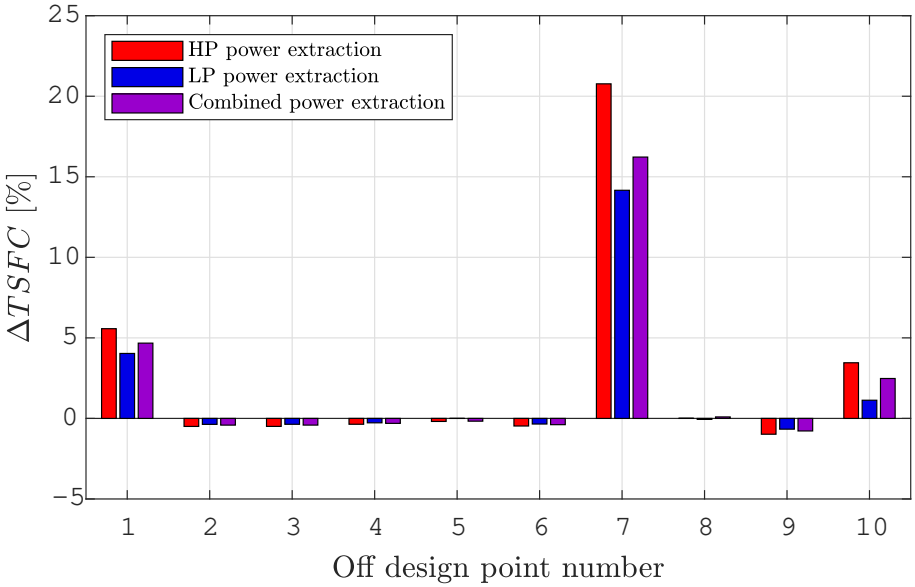

Figure 4.3: TSFC compared to Baseline [56].

The limitations introduced with large power extraction at military and maximum augmented power is best illustrated with performance plots for a range of subsonic and supersonic Mach numbers. Figures 4.5–4.12 present F_N, T_4, π_c and SFC variations with θ_0 for Mach numbers ranging from 0.5 to 2.0 at an altitude of 9 km. In Figure 4.5, the net thrust variation with θ_0 is shown. A similar illustration of the maximum augmented net thrust is provided in Figure 4.6. A significant break point can be observed at the θ_0 break, $\theta_0 = 1.1$ for the reference case, after which the increase in thrust with θ_0 diminishes. Figures 4.5 and 4.6 confirm the previous observation that the most significant thrust drop is associated with the extraction of power from the HP shaft at higher velocities and hence higher inlet temperatures. Figures 4.7 and

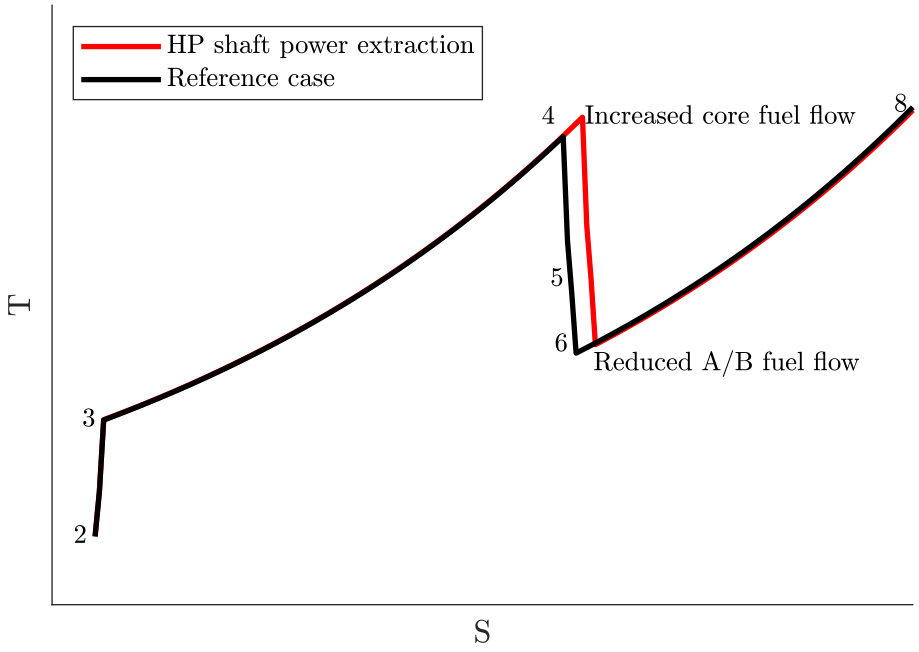

Figure 4.4: Schematic T-S diagram, reference case and HP shaft power extraction illustrated [56]. The figure is based on Figure 8 in [55].

4.8 show that the engine reaches its maximum T_4 at a lower velocity when power is extracted from the HP shaft. Beyond this velocity, the engine must be throttled down as illustrated in Figures 4.9 and 4.10. The θ_0 break is therefore moved to the left.

The SFC variation with θ_0 is shown for the military power case in Figure 4.11 and for the maximum augmented case in Figure 4.12. At military power, power extraction causes an increase in SFC in the evaluated range of θ_0/Mach numbers. The general trend for the maximum augmented power case is also an increase in SFC, although a slight improvement of the HP extraction case for $\theta_0 < \theta_{0,break}$ may be possible if a T_4 increase is acceptable, as discussed above.

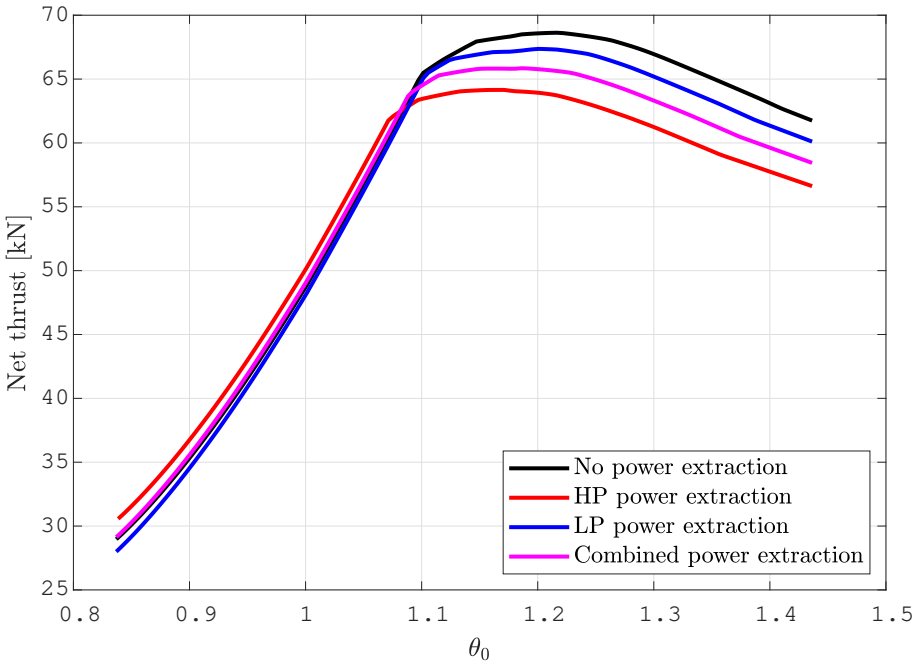

Figure 4.5: F_N variation with θ_0, at an altitude of 9 km and military power [56].

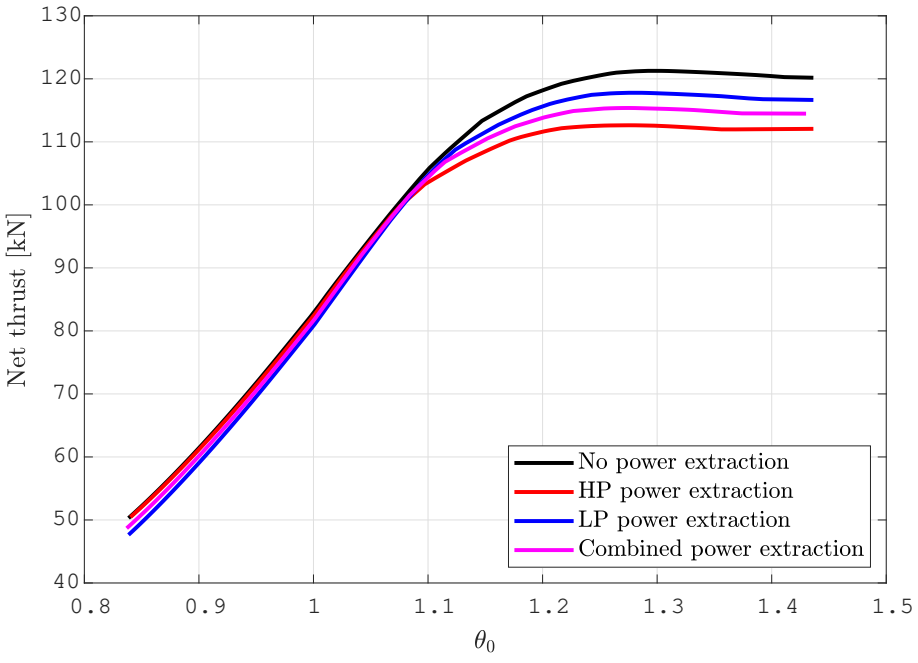

Figure 4.6: F_N variation with θ_0, at an altitude of 9 km and maximum augmented power [56].

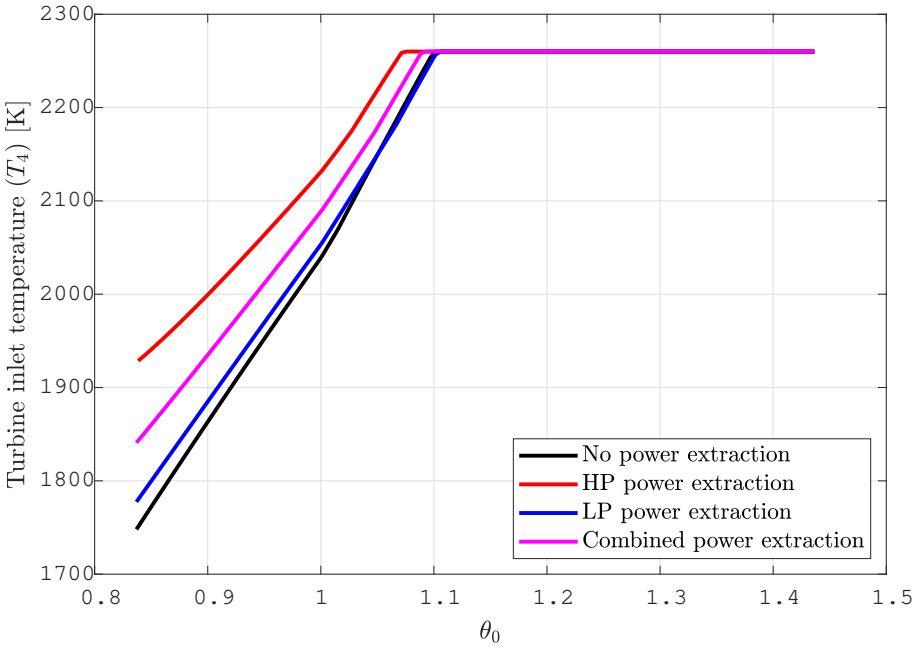

Figure 4.7: T_4 variation with θ_0, at an altitude of 9 km and military power [56].

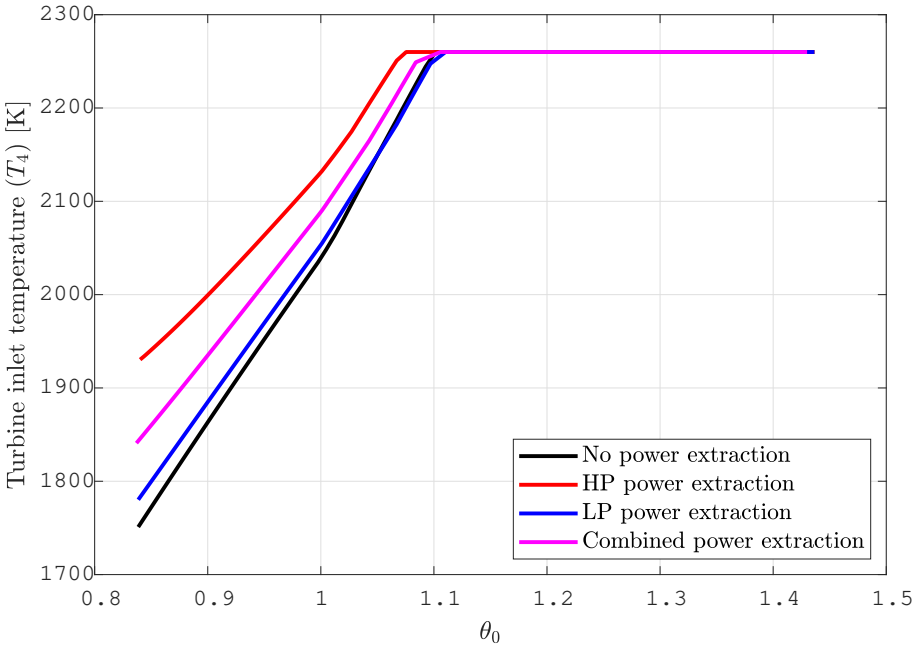

Figure 4.8: T_4 variation with θ_0, at an altitude of 9 km and maximum augmented power [56].

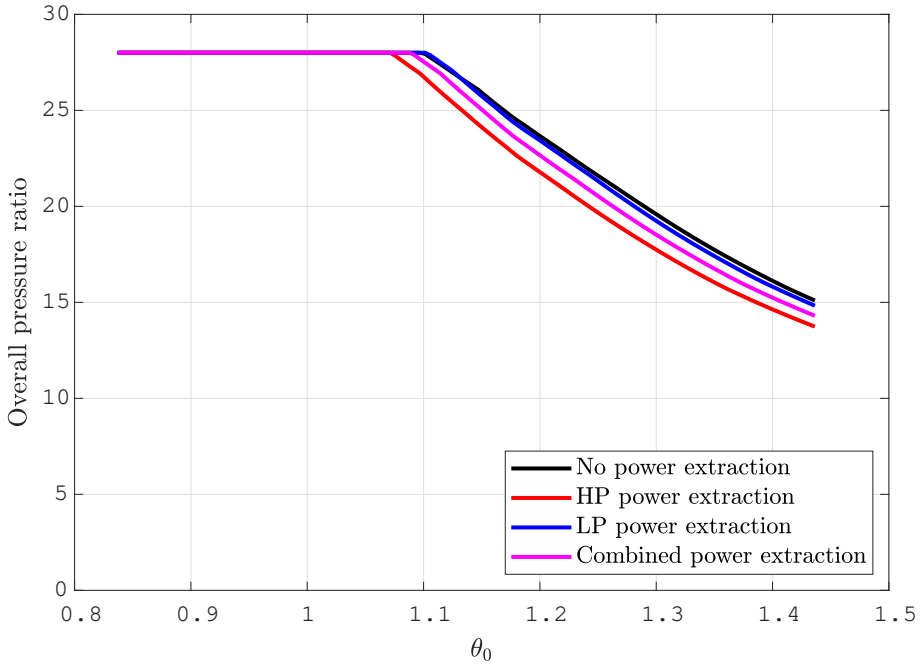

Figure 4.9: π_c variation with θ_0, at an altitude of 9 km and military power [56].

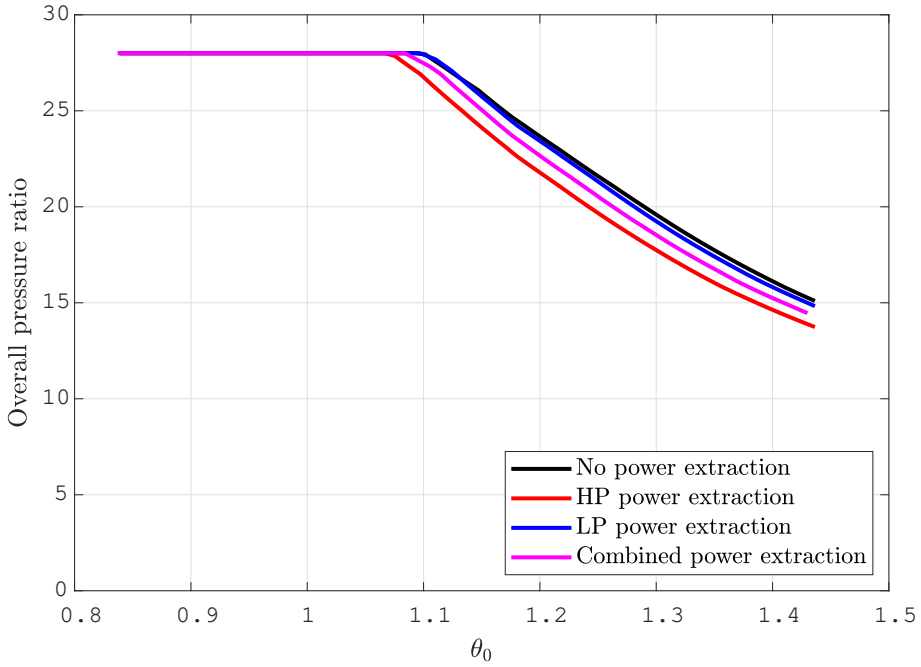

Figure 4.10: π_c variation with θ_0, at an altitude of 9 km and maximum augmented power [56].

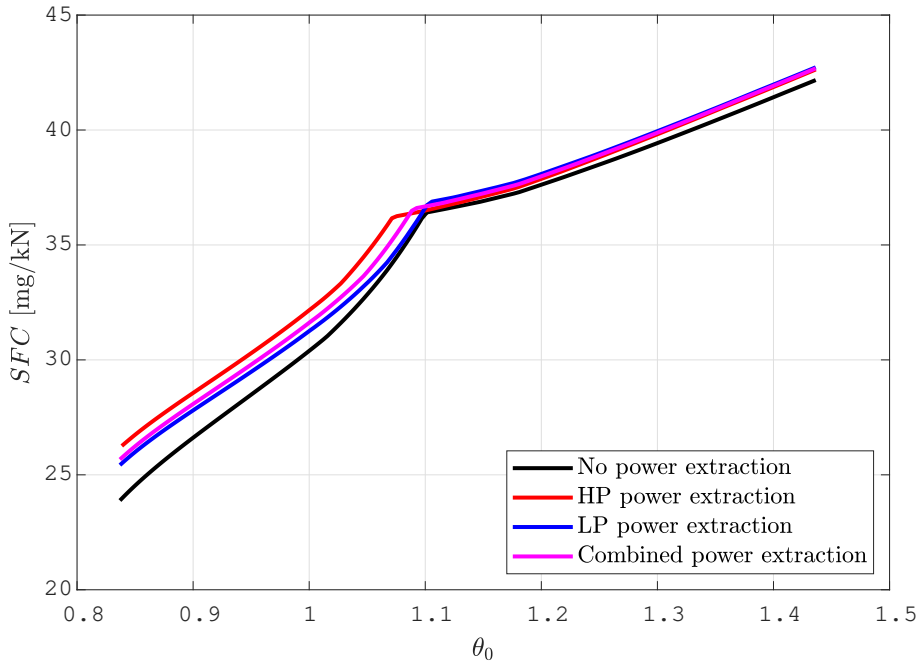

Figure 4.11: SFC variation with θ_0, at an altitude of 9 km and military power [56].

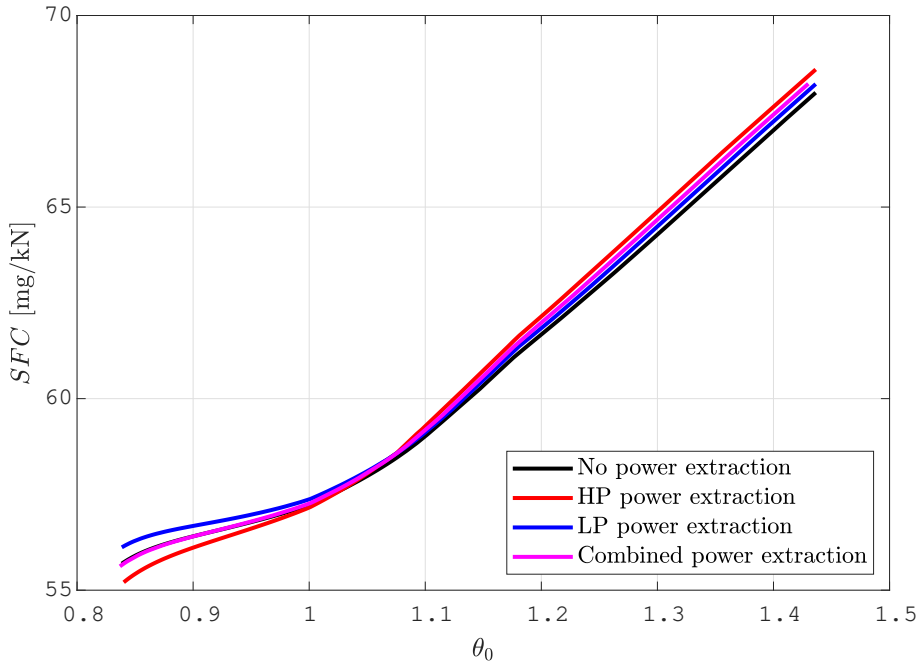

Figure 4.12: SFC variation with θ_0, at an altitude of 9 km and maximum augmented power [56].

4.2 FLADE turbofan engine evaluation

The FLADE turbofan engine concept is an attempt to improve the subsonic performance of a high-performance fighter aircraft with high supersonic speed capabilities by introducing a FLADE and an additional bypass duct to an existing low-bypass-ratio mixed-flow turbofan engine. Although the quest for improved maneuverability and increased supersonic speeds calls for increased maximum performance of the engine, such throttled-back subsonic cruise conditions constitute a majority of the operating time of a typical combat aircraft mission [4]. Thus, there is much to be gained from a reduced fuel consumption in cruise and loiter phases of a mission.

Different phases of the mission presented in Section 2.1 are used to evaluate the performance of the aircraft with the conventional turbofan engine and the FLADE turbofan engine. To achieve an adequate comparison, both part-power and maximum power performance of the two concepts are evaluated. In aircraft simulations, engine performance for the different engine alternatives is represented by a large number of simulations, covering several thrust levels ranging from low part-power settings up to maximum augmented power for each point in the flight envelope, as illustrated in Table 4.2.

Table 4.2: Engine performance data summary.

Engine configuration	**Turbofan engine**	**FLADE turbofan engine**
Design point α_{core}	0.25 0.5	0.25 0.5
FLADE flow restriction	– –	Miminum flow No flow restriction
Altitudes [km]	0.0 0.5 1.0 ... 15.0	0.0 0.5 1.0 ... 15.0
Mach numbers	0.425 0.475 0.525 ... 2.325	0.425 0.475 0.525 .... 2.325
Power settings	Part ↓ Military ↓ Partly augmented ↓ Maximum augmented	Part ↓ Military ↓ Partly augmented ↓ Maximum augmented

An aircraft weight penalty is added to the FLADE turbofan engine for each phase, corresponding to the additional weight associated with this engine alternative.

If an engine concept like the FLADE turbofan engine provides fuel savings, the fuel required to complete a certain mission will be reduced. This can actually provide weight savings at the aircraft level. However, this study was carried out as an aircraft reengineering study in which any improvements in engine performance are used to improve aircraft capabilities. In this way, advantages and disadvantages of the FLADE turbofan engine concept are illustrated more clearly.

An additional parasite drag penalty is applied to the FLADE turbofan engine due to its increased cross-sectional area, which results from the added bypass duct. Similarly to the weight estimation, this may be an overly pessimistic assumption. As stated in Section 3.5, the FLADE turbofan engine has the potential to improve the thermal management of the aircraft. If so, some volume and weight of existing aircraft cooling systems may be spared. Various methods are already being evaluated to reduce the weight and volume of these cooling systems [26, 125–127]. However, for this pure performance study, such potential volume or weight savings of the aircraft were not taken into account.

The additional weight and drag in combination with the minimum flow limitation described in Section 3.5 reduces the maximum performance of the aircraft in some parts of the flight envelope. Although this is primarily intended as a reengineering study to improve the fuel efficiency of an existing engine at the expense of such performance degradation, an option would be to connect the FLADE to a higher specific thrust engine, with improvements in maximum engine performance but a fuel efficiency equivalent to a conventional turbofan engine with lower specific thrust. As an example of such a high specific thrust engine, a conventional turbofan engine with a core bypass ratio $\alpha_{core} = 0.25$ was evaluated alongside the DP2 engine with $\alpha_{core} = 0.5$. To evaluate the impact of the minimum flow limitation separately, an engine with complete shut-off capability of flow to the FLADE duct was also investigated.

The subsonic performance of the concept is analyzed for the initial subsonic cruise segment, Phase 3 of the mission given in Figure 2.2. It is evaluated for an initial and a late phase of the segment with aircraft weight fractions $\beta = 0.96$ and $\beta = 0.76$. Figure 4.13 illustrates the specific range R_s in the flight envelope, for a turbofan engine and a FLADE turbofan engine with a core bypass ratio $\alpha_{core} = 0.5$ in the two phases. A similar illustration is provided in Figure 4.14 for a core bypass ratio $\alpha_{core} = 0.25$. The improvement in range with the FLADE turbofan engine is 3.7–4.0% at the optimal cruise point [77]. This improvement is due to a reduction in spillage drag and an improvement in propulsive efficiency. More significant performance improvements are possible in the lower right part of the subsonic flight envelope, where the potential reduction in spillage drag is even greater. These improvements seem realistic compared to the estimated improvements that have been reported for similar VCEs for military applications [90]. Figures 4.13 and 4.14 also show that a fuel consumption equivalent to the conventional turbofan engine with a moderate core bypass ratio (α_{core}) can be achieved with an engine with a lower core bypass ratio ($\alpha_{core} = 0.25$), if equipped with a FLADE. This opens up the advantages that such an engine offers at, for example, high speed without compromising the fuel efficiency of subsonic cruise phases.

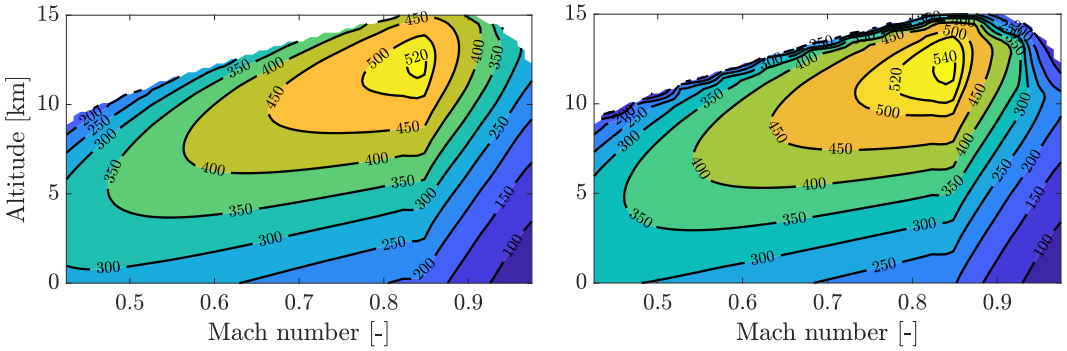

(a) Turbofan R_s, $\beta = 0.96$ [77].

(b) FLADE turbofan R_s, $\beta = 0.96$ [77].

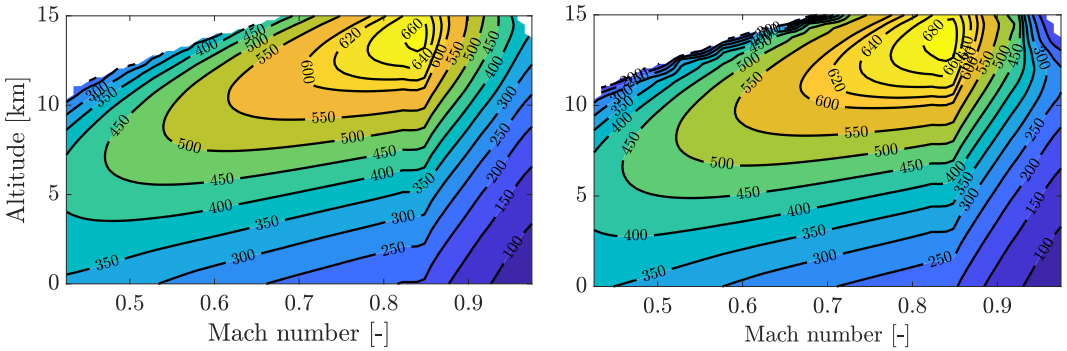

(c) Turbofan R_s, $\beta = 0.76$.

(d) FLADE turbofan R_s, $\beta = 0.76$.

Figure 4.13: Specific range comparison over the flight envelope. $\alpha_{core} = 0.5$ [77].

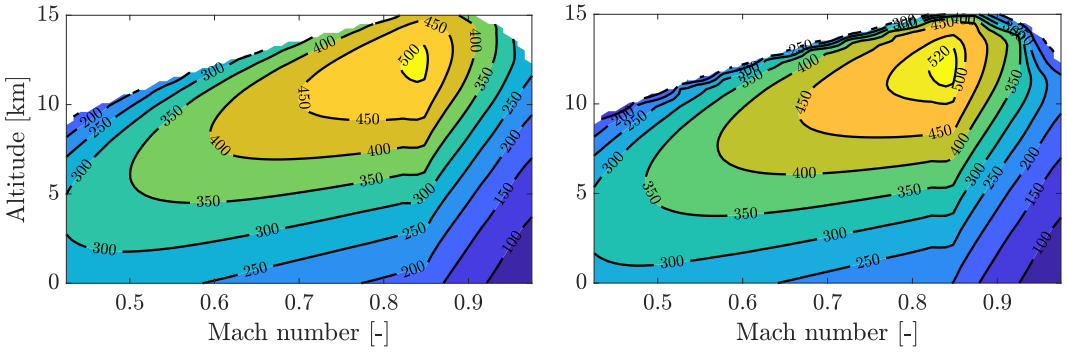

(a) Turbofan R_s, $\beta = 0.96$ [77].

(b) FLADE turbofan R_s, $\beta = 0.96$ [77].

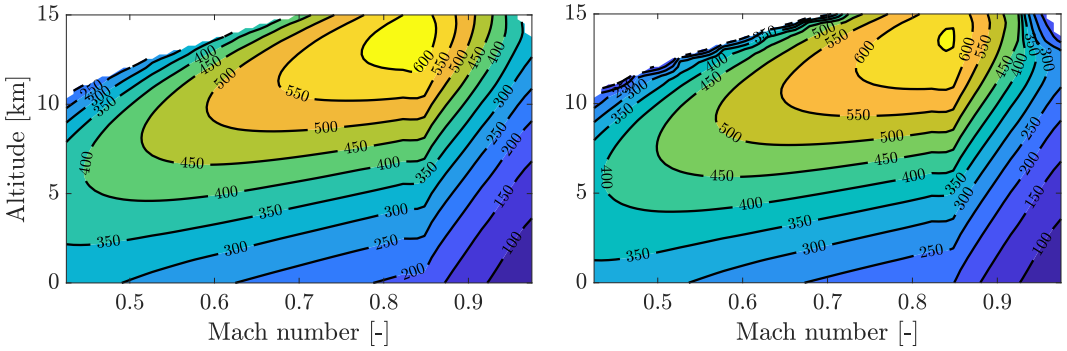

(c) Turbofan R_s, $\beta = 0.76$.

(d) FLADE turbofan R_s, $\beta = 0.76$.

Figure 4.14: Specific range comparison over the flight envelope. $\alpha_{core} = 0.25$ [77].

The optimum speed for loiter is lower compared to the optimal cruise point. This reduces the potential for spillage drag reduction compared to the cruise case. Figures 4.15 and 4.16 show the loiter performance over the flight envelope for the core bypass ratios $\alpha_{core} = 0.5$ and $\alpha_{core} = 0.25$. The improvement in specific endurance for the FLADE turbofan engine compared to the conventional turbofan engine is 1.9–2.4% [77].

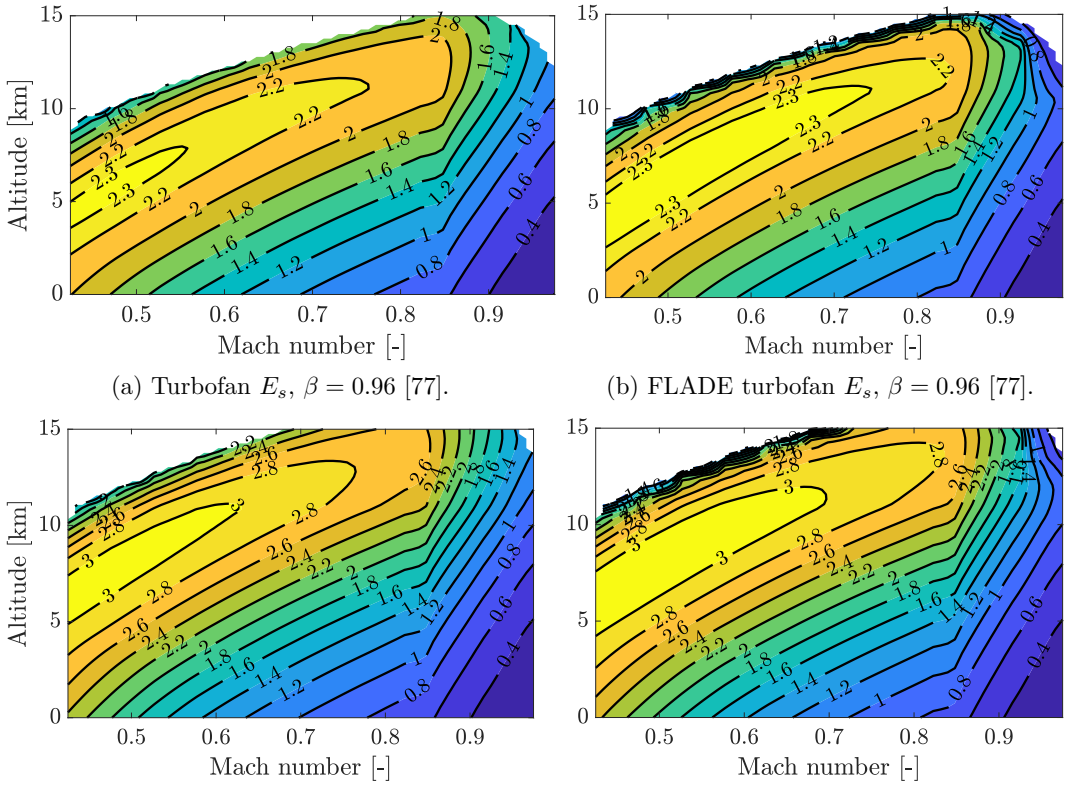

(a) Turbofan E_s, $\beta = 0.96$ [77].

(b) FLADE turbofan E_s, $\beta = 0.96$ [77].

(c) Turbofan R_s, $\beta = 0.76$.

(d) FLADE turbofan E_s, $\beta = 0.76$.

Figure 4.15: The specific endurance over the flight envelope with $\alpha_{core} = 0.5$ [77].

Further improvements of the specific range can be achieved with a wider FLADE duct as illustrated in Figure 4.17. If the duct area is increased from 20% to 40% of the fan annulus area, an improvement in TSFC of 0.5–1.0% can be achieved for typical cruise and loiter phases. On the other hand, such an increase in area will have negative consequences for the supersonic performance of the aircraft. A high-speed configuration, with a FLADE duct area corresponding only to 15% of the fan annulus area is also illustrated in Figure 4.17. However, this narrow area of the FLADE duct will cause substantial losses, as was shown in Figure 3.9. Such high losses will cancel many of the performance benefits introduced by the FLADE. The increase in TSFC is approximately 1.0–1.5% in cruise and loiter, as illustrated in Figure 4.17.

The escape dash, Phase 6 of the mission in Figure 2.2 with an aircraft weight fraction $\beta = 0.65$, was used to evaluate the maximum performance of the different engine alternatives. Figure 4.18 demonstrates the impact of different engine concepts on the acceleration of the aircraft.

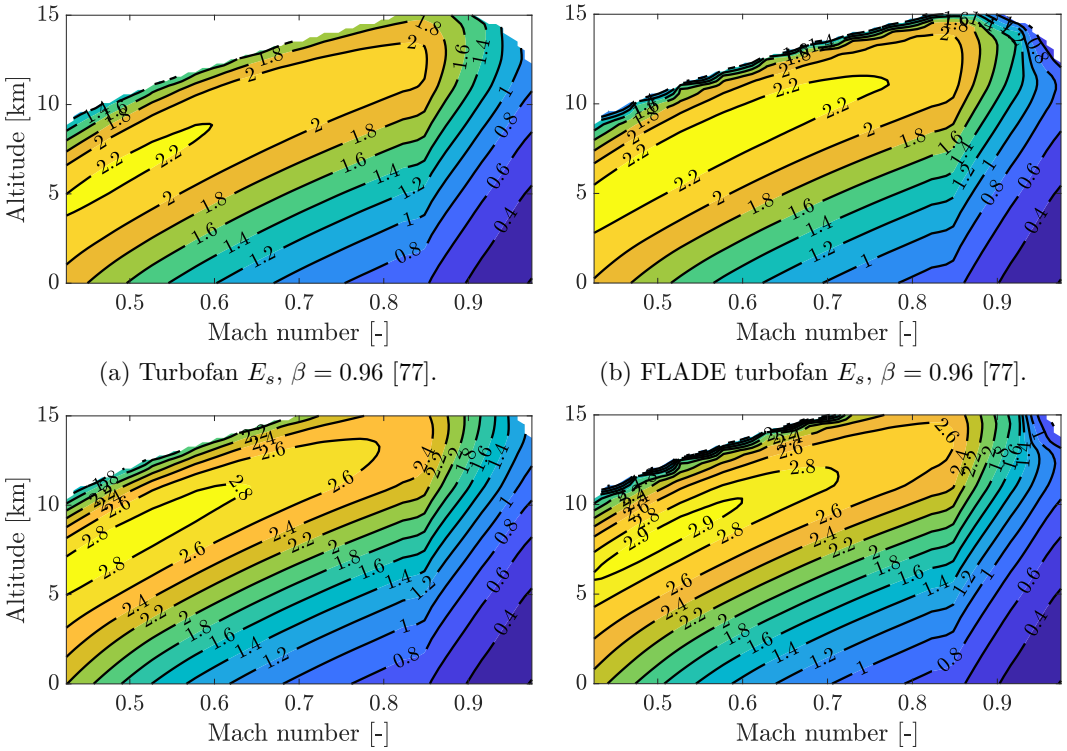

(a) Turbofan E_s, $\beta = 0.96$ [77].

(b) FLADE turbofan E_s, $\beta = 0.96$ [77].

(c) Turbofan E_s, $\beta = 0.76$.

(d) FLADE turbofan E_s, $\beta = 0.76$.

Figure 4.16: The specific endurance over the flight envelope with $\alpha_{core} = 0.25$ [77].

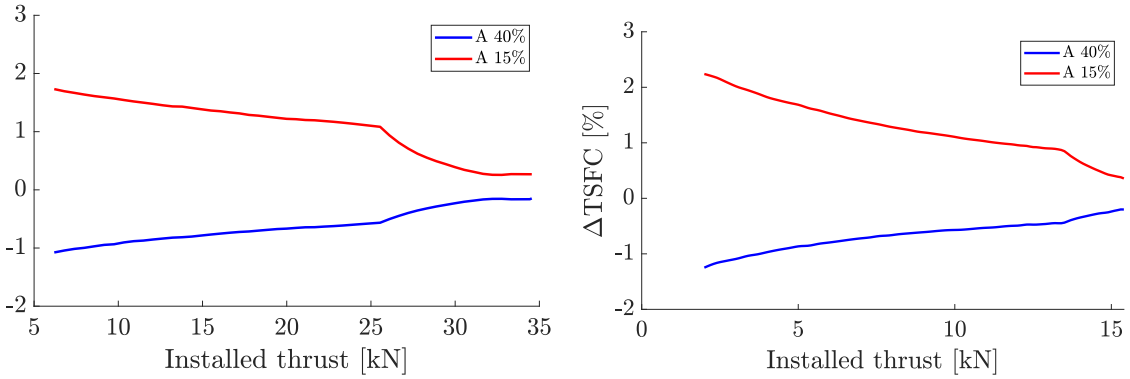

(a) Relative TSFC change with different duct areas in a loiter point. Altitude 5.7 km, 0.48 M.

(b) Relative TSFC change with different duct areas in a cruise point. Altitude 12 km, 0.84 M.

Figure 4.17: Duct area impact on TSFC [77].

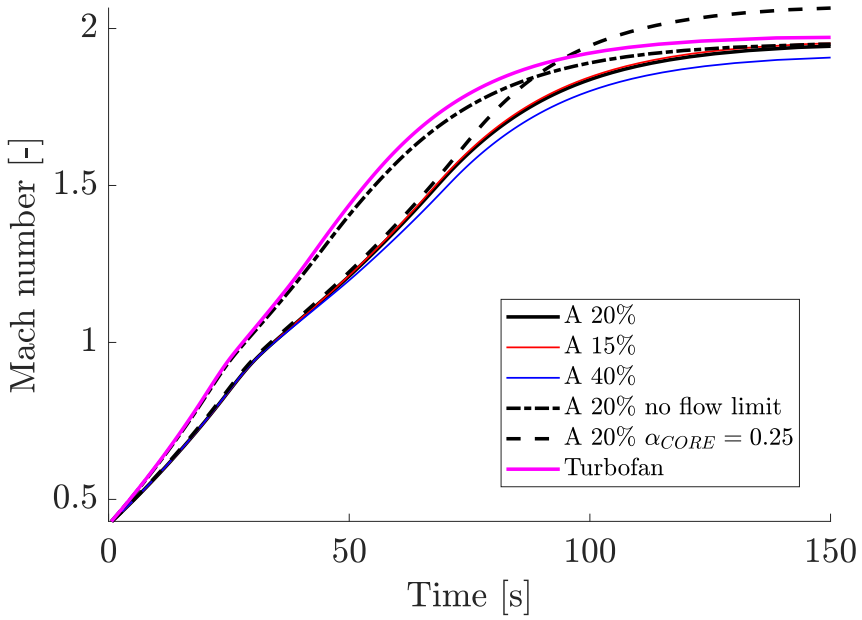

Figure 4.18: Acceleration performance of different configurations [77].

Figure 4.18 shows that the acceleration time of the aircraft with the FLADE turbofan engine, illustrated with the solid black curve, increases compared to the conventional turbofan engine. The increase in acceleration time is mainly due to the minimum flow requirement of the FLADE, which reduces the maximum flow to the turbofan engine. This is evident from the dash-dotted curve of Figure 4.18, illustrating the FLADE turbofan engine without flow restriction, which exhibits an acceleration performance almost equivalent to the conventional turbofan engine. The limitations in acceleration performance are of course most significant in parts of the flight envelope where the maximum power of the engine is already restricted by airflow limitation, i.e. at lower flight velocities. In high-speed flight, the FLADE turbofan engine's ability to reduce spillage drag compensates for the negative impact from increased cross-sectional area and the increased weight of the engine. From Figure 4.18 it can be concluded that the reduction in the FLADE duct area from 20% to 15% of the fan annulus area (red curve) provides very little improvement in the acceleration time of the aircraft. Given the considerable increase in fuel consumption at part-power, this reduction in the FLADE duct area is difficult to justify. Increasing the FLADE duct area to 40% of the annulus area of the fan (blue curve) has a significant negative impact, both on the acceleration time and the maximum speed of the aircraft. Such a wide duct could possibly be justified for an aircraft designed for a mission with a clear predominance of subsonic flight phases. Finally, from Figure 4.18, it can be concluded that improvements can be achieved at maximum power if the thermodynamic cycle of the turbofan engine is negotiable. An increase in maximum speed with the FLADE turbofan engine is achieved with $\alpha_{core} = 0.25$. As noted above, this engine alternative provides a subsonic part-power fuel efficiency comparable to that of a conventional turbofan engine with $\alpha_{core} = 0.5$. The cycle design and TR of the $\alpha_{core} = 0.25$ turbofan engine was selected in favor of

high speed capability. By making other choices for the thermodynamic design cycle and the control schedules of the turbofan engine, these performance benefits can of course be transferred to other regions of the flight envelope.

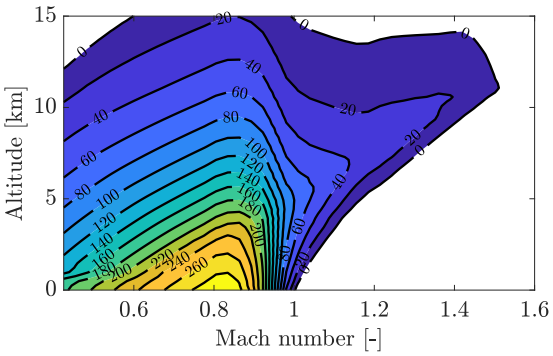

(a) Turbofan P_s. Military power.

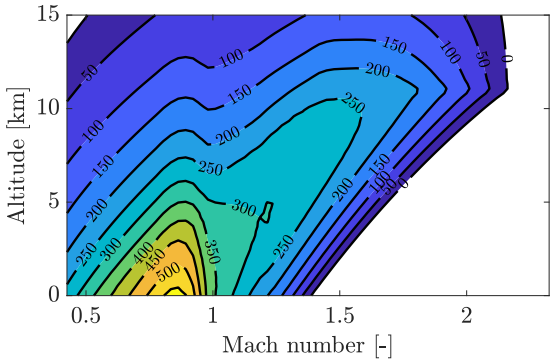

(b) Turbofan P_s. Maximum augmented power.

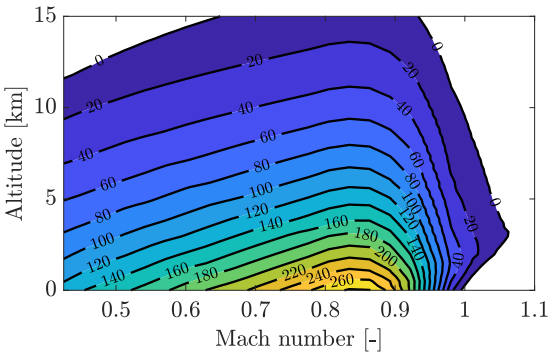

(c) FLADE turbofan P_s. Military power.

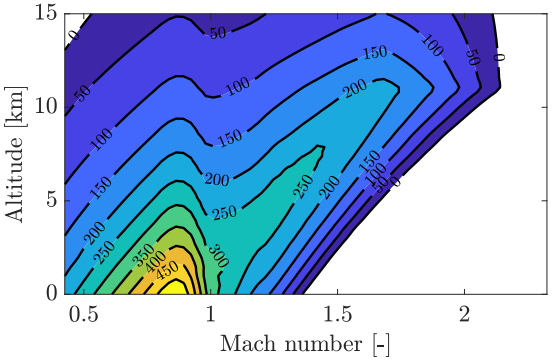

(d) FLADE turbofan P_s. Maximum augmented power.

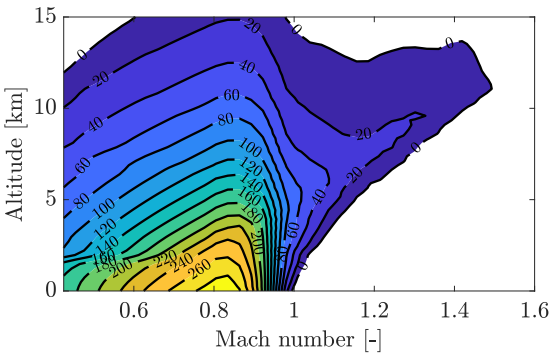

(e) FLADE turbofan P_s. Military power with no flow limitation.

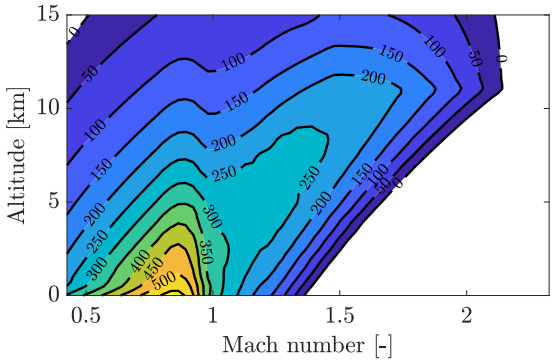

(f) FLADE turbofan P_s. Maximum augmented power, no flow limitation.

Figure 4.19: Comparison of specific excess power with $\beta = 0.65$ [77].

We can expand the view to include the entire flight envelope for both military and maximum augmented power, as illustrated in Figure 4.19. Even if not specified in the design mission in Section 2.1, an unfortunate disadvantage of the FLADE turbofan engine is that the supercruise capability, that is, supersonic flight without the use of afterburner, is lost for this aircraft/engine configuration. As illustrated

in Figure 4.19c ($P_s < 0$), this is mainly due to the minimum flow requirement of the FLADE at military power. If all flow was available for the turbofan engine, the supercruise capability would be preserved. This is also shown in Figure 4.19e.

Chapter 5

Summary of Papers

5.1 Paper 1

Daniel Rosell and Tomas Grönstedt. *Design Considerations of Low Bypass Ratio Mixed Flow Turbofan Engines with Large Power Extraction.* Fluids 2022, 7(1), 21.

5.1.1 Division of work

Both authors contributed to conceptualization, methodology, software, and validation while the formal analysis was performed by the author of the thesis. The author of the thesis performed the simulations, post-processed the results, and wrote the original draft of the paper. Tomas Grönstedt contributed with feedback on the manuscript.

5.1.2 Aim

In low-bypass-ratio mixed-flow turbofan engines, power is normally extracted from the HP shaft. The aim of the work was to evaluate how the performance of a typical low-bypass-ratio mixed-flow turbofan engine is affected by large power extraction from the HP shaft in different parts of a fighter mission. This type of engine performance study, related to large power extraction, has not previously been conducted for low-bypass-ratio mixed-flow turbofan engines.

5.1.3 Research question

How does large power extraction from the HP shaft affect the performance of a low-bypass-ratio mixed-flow turbofan engine in terms of net thrust and specific fuel consumption in different parts of a typical fighter aircraft mission?

5.1.4 Methodology description

A low-bypass-ratio mixed-flow turbofan engine was modeled in GESTPAN and simulations were performed in key points of a fighter mission to illustrate the

performance impact in different parts of the flight envelope and with different power levels of the engine. The mission points were simulated with an engine power extraction of 900 kW, extracted from the HP shaft. These results were compared to the baseline case without power extraction from the engine.

5.1.5 Discussion

The study illustrated that the performance impact of large power extraction from the HP shaft will depend on flight altitude and speed, but also on engine power level. The large extraction of power from the HP shaft will result in an increase in the turbine inlet temperature (T_4). If the engine runs at high power and the temperature increase is acceptable from an engine operability point of view, power extraction from the HP shaft will have limited impact on the specific fuel consumption and net thrust of the engine. On the other hand, if the engine is operating at, or close to, its maximum turbine inlet temperature limit, the thrust reduction will be quite substantial. This is illustrated in Section 4.1.

5.2 Paper 2

Daniel Rosell, Tomas Grönstedt, Pedro David Bravo-Mosquera, Fernando Martini Catalano. *Low BPR Turbofan Performance with Power Extraction.* 33rd Congress of the International Council of the Aeronautical Sciences, Stockholm, Sweden, 2022, 6, 4382.

5.2.1 Division of work

The author of the thesis and Tomas Grönstedt contributed to the conceptualization, the methodology, the engine modeling software and the validation. The formal analysis was performed by the author of the thesis. Pedro David Bravo-Mosquera and Fernando Martini Catalano provided the software for the aircraft model. The author of the thesis performed the simulations, post-processed the results and wrote the original draft of the paper. Section 2.1, which describes the conceptual design of the aircraft, was written by Pedro David Bravo-Mosquera and added to this original draft. Pedro David Bravo-Mosquera defined a mission, carried out the conceptual design of the aircraft, and provided the mission thrust requirements for the engine. Tomas Grönstedt reviewed the manuscript and provided feedback.

5.2.2 Aim

To accommodate the increasing power demand of various aircraft systems, an alternative to extracting all power from the HP shaft is to extract part or all of the required power from the LP shaft. In Paper 2, the study conducted in Paper 1 was expanded to also include power extraction from the LP shaft, as well as a combination of power extraction from the HP and the LP shaft. The aim of Paper 2 was to evaluate the impact on engine performance of large power extraction when both the HP and LP

shafts are available for power extraction. Large power extractions from different shafts have previously been evaluated for high-bypass-ratio turbofan engines, but not for low-bypass-ratio mixed-flow turbofan engines.

5.2.3 Research question

How does large power extraction from the HP shaft, the LP shaft, or a combination of the two shafts affect the performance of a low-bypass-ratio mixed-flow turbofan engine in terms of net thrust and specific fuel consumption in different parts of a typical fighter aircraft mission?

5.2.4 Methodology description

The modeled low-bypass-ratio mixed-flow turbofan engine was adapted to allow power extraction also from the LP shaft and used to evaluate the performance impact of large power in the different mission points. Four cases were evaluated. A first option with 900 kW power extraction from the HP shaft, a second option with 900 kW power extraction from the LP shaft, and a third option with a combined power extraction of 450 kW from each shaft were simulated and compared with the baseline case.

5.2.5 Discussion

The analysis identified a considerable difference in the impact on engine performance when the LP shaft was introduced as an option for power extraction. Power extraction from the HP shaft was shown to cause the worst thrust drop when the engine was operating at or close to the turbine inlet temperature limit (T_4). If the engine is limited by the OPR limitation, extraction of power from the LP shaft will cause the worst thrust drop. The analysis showed that power extraction from different shafts can be beneficial in different parts of the flight envelope and at different power levels of the engine depending on the flight case concerned. This is shown in Section 4.1.

5.3 Paper 3

Daniel Rosell, Tomas Grönstedt. *Aircraft Performance Impact with a Turbofan Engine Using a Fan on Blade.* Journal of Propulsion and Power, 2026, 42(3), 392.

5.3.1 Division of work

Both authors contributed to conceptualization, methodology, engine modeling software, and validation. Tomas Grönstedt implemented the FLADE component in the GESTPAN performance code as described in [42]. A refined FVG was developed, based on a previous GESTPAN performance code, by both authors to control the FLADE flow, and both authors contributed to the development of the FLADE bypass duct. The schedules for FVG and FLADE nozzle control was developed by

the author of the thesis. Tomas Grönstedt performed an update to the WEICO weight estimation model to be able to calculate the weight of the FLADE turbofan engine and the conventional turbofan engine. The weight calculations, based on the specific design parameters, were performed by the author of the thesis. The aircraft performance model, used for aircraft performance evaluation, was developed by the author of this thesis.

The formal analysis was conducted by the thesis author, who also prepared the original draft of the paper. Tomas Grönstedt reviewed the draft and provided feedback and suggestions for improvement.

5.3.2 Aim

The aim of Paper 3 was to evaluate how the performance of a fighter aircraft with a low-bypass-ratio mixed-flow turbofan engine is affected if the engine is equipped with a FLADE, providing an additional bypass flow through a separate bypass duct and exhaust nozzle. Unlike previous studies on the FLADE turbofan engine, this study covers the aircraft and engine performance over a wide operating range of the aircraft.

5.3.3 Research question

How is the performance of a fighter aircraft affected across the flight envelope and in different phases of a mission if it is equipped with a low-bypass-ratio mixed-flow turbofan engine fitted with a FLADE?

5.3.4 Methodology description

A FLADE was integrated with a low-bypass-ratio mixed-flow turbofan engine model. Aircraft performance simulations were performed, both for the FLADE turbofan engine and for the conventional turbofan engine. The two concepts were compared in terms of aircraft performance, with parameters such as specific range, specific endurance, aircraft acceleration, and specific excess power.

5.3.5 Discussion

Integrating a FLADE with a conventional low-bypass-ratio mixed-flow offers improvements in terms of reduced spillage drag of the engine and increased range of the aircraft. However, if the FLADE requires a minimum flow, this will limit the military power and the maximum augmented power of the engine. This will in turn affect the performance of the aircraft in some parts of the flight envelope, as illustrated in Section 4.2.

5.4 Paper 4

Emil Ellenius, Tomas Grönstedt, Daniel Rosell. *Aerodynamic Design of Fan on Blade for Multiple Operating Points.* Submitted to The Aeronautical Journal, 2026.

5.4.1 Division of work

Emil Ellenius and Tomas Grönstedt performed the conceptualization and developed the methodology. Emil Ellenius performed the investigation, the data curation, and the validation while formal analysis was carried out by all authors. The author of the thesis provided the sizing conditions and requirements for the FLADE based on calculations of aircraft and engine performance, reviewed the draft version, and contributed the article with visualization.

5.4.2 Aim

The aim of Paper 4 is to benchmark the performance of two designs across five typical operating points.

5.4.3 Methodology description

Output from the performance simulations is used as input for the designs created and evaluated using computational fluid dynamics (CFD).

5.4.4 Discussion

Two designs were proposed and evaluated based on the performance calculations.

Chapter 6

Conclusions

For future fighter aircraft, engines are being sought that can meet the high thrust requirements of challenging maneuvers, at the same time provide high fuel efficiency in subsonic flight, and beyond that supply an increasing amount of power for aircraft systems. Engines used in combat aircraft are usually two-spool low-bypass-ratio turbofan engines, where mechanical shaft power could be extracted from the LP shaft, the HP shaft, or potentially from both shafts. In this work, the impact on engine performance from large power extraction was investigated. An increase in fuel consumption and turbine inlet temperature is required to meet such large power demands, regardless of whether the power is extracted from the LP or the HP shaft. However, the increase in turbine inlet temperature will be greater when power is extracted from the HP shaft. Increasing the turbine inlet temperature increases the specific thrust of the engine. Such an increase in specific thrust results in an increase in specific fuel consumption at part-power conditions due to the reduction in propulsive efficiency but may be beneficial in afterburner operation if a power redistribution from the less efficient afterburner to the main combustor can be achieved.

In high-speed operation, when the engine approaches the maximum turbine inlet temperature, this higher turbine inlet temperature increase associated with HP shaft power extraction significantly reduces the maximum thrust of the engine. In these flight cases, when the engine operates at the maximum turbine inlet temperature, extraction of power from the LP shaft has a less limiting effect on maximum thrust of the engine.

Potential improvements in engine performance at military power or maximum augmented power with HP shaft power extraction have been revealed in the upper left part of the flight envelope, where the engine is limited by the maximum π_c, but this improvement comes with a shift towards surge of the HPC operating line. Unfortunately, this is a part of the flight envelope where increased sensitivity to power off-takes can be expected, in terms of engine operability.

The flexibility of VCEs might offer solutions to these challenges with regard to operability and large power off-takes, and also the dissipation of heat generated from power-consuming equipment. The downside of VCEs is the increased weight and complexity, but also the risks associated with a VCE development program

and the costs that might emerge due to maintenance of an increased number of engine components. In this work a less complex VCE, referred to as the FLADE turbofan engine, was studied. It has many of the advantages of a more sophisticated VCE, but requires fewer additional components and can be adapted to an existing turbofan engine. The changes required for the design and control of the turbofan engine should be more moderate. Together, this should reduce the risk and cost associated with the development program for a FLADE turbofan engine. Since this simpler concept had previously been studied only to a limited extent, it warranted further investigation.

The study showed that improvements in the subsonic part-power performance can be achieved if a FLADE is connected to the fan of a conventional low-bypass-ratio mixed-flow turbofan engine, to establish an additional bypass stream circumscribing the turbofan engine. This outer bypass flow improves the propulsive efficiency of the engine and reduces the intake spillage drag in subsonic part-power operating cases, such as cruise and loiter. For the aircraft/engine configuration studied, an approximate range improvement of 4% and a loiter endurance improvement of around 2% are achieved, with the additional weight of the engine taken into account. This improvement comes at the expense of a reduction in maximum performance in certain parts of the flight envelope due to the minimum flow requirement of the FLADE, which reduces the maximum flow available for the turbofan engine. If this minimum flow could be shut off, a maximum performance close to that of the conventional turbofan engine can be achieved in the parts of the flight envelope concerned. The slight reduction in aircraft performance due to the moderate increase in engine weight and cross-sectional area will be compensated for by the reduction in spillage drag provided by the FLADE turbofan engine in high-speed flight. Although a more advanced VCE might yield further performance improvements, this would come at the expense of increased weight and complexity.

It can be discussed whether the pure performance comparison with the conventional turbofan engine conducted here is fair if the flow in the FLADE duct can be used for cooling purposes. If so, the minimum flow required by the FLADE turbofan engine does indeed result in some reduced maximum performance of the engine, but it also contributes a solution to the increasing problem of thermal management at the aircraft level, a problem that otherwise must be solved in another way. This alternative solution will, of course, also have an impact on the performance of the aircraft.

In conclusion, the FLADE turbofan engine can be an interesting alternative for a future fighter aircraft with requirements of high efficiency in subsonic cruise and loiter operation in combination with challenging demands for both subsonic maneuvering and supersonic high-speed flight, i.e., maximum speed well beyond 1.6 M. Such a high-speed aircraft can be difficult to design with a fixed intake and a conventional turbofan engine with satisfying supersonic performance without imposing considerable amounts of spillage drag to the installation. A common approach is to use intakes with variable geometry to better match the intake with the flow requirements at the different operating points of the engine. However, such intakes are both heavy and complex. Then, they also do not provide an additional

heat sink for the dissipation of excessive heat or contribute to engine thrust. Hence, the FLADE turbofan engine constitutes an interesting option for a high-speed fighter, reducing the need for a variable geometry intake.

Bibliography

1. Anderson JD. Aircraft performance and design. Vol. 1. WCB/McGraw-Hill Boston, 1999:293, 310, 314, 345, 348, 351, 521, 539–40 (cit. on pp. 3, 11–13).
2. Jenkinson LR and Marchman J. Aircraft design projects: for engineering students. Elsevier, 2003 (cit. on pp. 3, 4).
3. Olsson U. Aerospace Propulsion from Insects to Spaceflight. In: 2nd ed. Stockholm, Sweden: Volvo Aero Corporation, 2012:186, 289, 297, 388–90, 393–5, 412, 416, 432, 434, 479, 505 (cit. on pp. 3, 27, 29, 31).
4. Philpot M. Future Challenges for Powerplant Aerodynamic Integration in Combat Aircraft. The Aeronautical Journal 2001;105:335–43 (cit. on pp. 3, 4, 46).
5. Walters E, Amrhein M, O'Connell T, Iden S, Lamm P, Yerkes K, Wolff M, McCarthy K, Raczkowski B, Wells J, et al. INVENT modeling, simulation, analysis and optimization. In: *48th AIAA Aerospace Sciences Meeting Including the New Horizons Forum and Aerospace Exposition*. 2010:3 (cit. on pp. 3, 4).
6. Liersch CM, Schuette A, Moerland E, and Kalanja M. DLR project diabolo: An approach for the design and technology assessment for future fighter configurations. AIAA paper 2023-3515 2023:17 (cit. on pp. 3, 8, 24, 26).
7. Johnson J. Variable Cycle Engine Developments. In: *Developments in High-Speed-Vehicle Propulsion Systems*. Ed. by Murthy S and Curran E. Vol. 165. Progress in Astronautics and Aeronautics. Reston, VA: AIAA, 1996:115–6 (cit. on pp. 4, 6, 8, 25, 30, 33, 35).
8. Bowers DL and Tamplin G. Throttle-Dependent Forces. In: *Thrust and drag: Its Prediction and Verification*. Ed. by Covert EE. Vol. 98. AIAA, 1985:207–77 (cit. on pp. 4, 22, 24, 25).
9. Johnson JE. FLADE Gas Turbine Engine with Fixed Geometry Inlet. US Patent 7,395,657. 2008 (cit. on pp. 4, 31).
10. Wyatt DD. A Review of Supersonic Air Intake Problems. In: *Air Intake Problems in Supersonic Propulsion*. Ed. by Fabri J. New York: Pergamon Press, 1958:21–47 (cit. on pp. 4, 22).
11. Ferri A. Problems Related to Matching Turbojet Engine Requirements to Inlet Performances as Function of Flight Mach Number and Angle of Attack. In: *Air Intake Problems in Supersonic Propulsion*. Ed. by Fabri J. New York: Pergamon Press, 1958:48–62 (cit. on pp. 4, 23).

12. Hawkins J. YF-16 Inlet Design and Performance. Journal of Aircraft 1976;13:436–41 (cit. on p. 4).

13. Whitford R. Fundamentals of Fighter Design. In: 1st ed. Shrewsbury: Airlife Publishing Ltd, 2000:80–2 (cit. on p. 4).

14. Saravanamuttoo H, Rogers GFC, Straznicky P, Cohen H, and Nix A. Gas Turbine Theory. In: 7th ed. Harlow, United Kingdom: Pearson Education Limited, 2017:71, 101, 127–30, 407–8, 510, 558 (cit. on pp. 4, 22, 24, 27–29).

15. Kurzke J and Halliwell I. Propulsion and Power: an Exploration of Gas Turbine Performance Modeling. In: 1st ed. Cham, Switzerland: Springer International Publishing, 2018:12, 33, 34, 49, 97, 99. DOI: 10.1007/978-3-319-75979-1 (cit. on pp. 4, 7, 8, 25, 27, 29, 30, 40).

16. van Heerden ASJ, Judt DM, Jafari S, Lawson CP, Nikolaidis T, and Bosak D. Aircraft Thermal Management: Practices, Technology, System Architectures, Future Challenges, and Opportunities. Progress in Aerospace Sciences 2022;128:13 (cit. on pp. 4, 32).

17. Doman DB. Rapid mission planning for aircraft thermal management. In: *AIAA guidance, navigation, and control conference*. 2015:1076 (cit. on p. 4).

18. Rolls-Royce plc. The jet engine. 5th ed. The Technical Publication Department. Rolls-Royce plc, 1996:65 (cit. on pp. 4, 22).

19. Charrier JJ and Kulshreshtha A. Electric actuation for flight and engine control; evolution and current trend. In: *45th AIAA Aerospace Sciences Meeting and Exhibit*. 2007:1391 (cit. on p. 4).

20. Clark R, Shi M, Gladin J, and Mavris D. Design and analysis of an aircraft thermal management system linked to a low bypass ratio turbofan engine. J. Eng. Gas Turbines Power 2022;144 (cit. on p. 4).

21. Oyori H, Morioka N, Kakiuchi D, Shimomura Y, Onishi K, and Sano F. System design for the more electric engine incorporated in the electrical power management for more electric aircraft. Tech. rep. SAE Technical Paper, 2012 (cit. on p. 4).

22. Boglietti A, Cavagnino A, Tenconi A, and Vaschetto S. The safety critical electric machines and drives in the more electric aircraft: A survey. In: *2009 35th Annual Conference of IEEE Industrial Electronics*. IEEE. 2009:2587–94 (cit. on p. 4).

23. Rosero J, Ortega J, Aldabas E, and Romeral L. Moving towards a more electric aircraft. IEEE Aerospace and Electronic Systems Magazine 2007;22:3–9 (cit. on p. 4).

24. Eek M. On credibility assessment in aircraft system simulation. PhD thesis. Linköping University Electronic Press, 2016 (cit. on p. 4).

25. Palmberg S and Westroth S. Model-based concept development of system in UAV. 2020 (cit. on pp. 4, 5).

26. Drego A and Sören S. A System Integrator's Perspective on Vehicle System Evaluation at the Aircraft Concept Stage. In: *33rd Congress of the International Council of the Aeronautical Sciences*. Vol. 7. Bonn, Germany: Deutsche Gesellschaft für Luft- und Raumfahrt, 2022:6120–30 (cit. on pp. 4, 5, 47).

27. Mattingly JD, Boyer KM, and Ohain H von. Elements of Propulsion: Gas Turbines and Rockets. In: AIAA Education Series. edited by J.A.Schetz. Reston, VA: AIAA, 2006:27 (cit. on pp. 5, 27, 29).

28. Lewis G. The next European engine for combat aircraft. The Aeronautical Journal 1984;88:1–9 (cit. on pp. 5, 27–29).

29. Kurzke J. The Mission Defines the Cycle: Turbojet, Turbofan and Variable Cycle Engines for High Speed Propulsion. NATO Research and Technology Organisation, RTO-EN-AVT-185-02, Dachau, Germany. 2010 (cit. on pp. 5, 7, 27, 29).

30. Demel HF. Installation of electric generators on turbine engines. NASA. Lewis Research Center Aircraft Elect. Secondary Power 1983:73–8 (cit. on p. 5).

31. Richter E and Neumann T. Jet Engine Integrated Generator. Journal of Energy 1982;6:45–8 (cit. on pp. 5, 7).

32. Chapman JW. A Study of Large Scale Power Extraction and Insertion on Turbofan Performance and Stability. In: *2020 AIAA/IEEE Electric Aircraft Technologies Symposium (EATS)*. IEEE. 2020:1–17 (cit. on p. 5).

33. Zähringer C, Stastny K, and Ardey S. Towards the powerhouse for more electric aircraft–dedicated engine concepts. In: *Proceedings of the 19th International Symposium on Air Breathing Engines*. 2009 (cit. on p. 5).

34. Pluijms A, Schmidt KJ, Stastny K, and Chibisov B. Performance comparison of more electric engine configurations. In: *Turbo Expo: Power for Land, Sea, and Air*. Vol. 43116. 2008:113–22 (cit. on p. 5).

35. Culley DE, Kratz JL, and Thomas GL. Turbine Electrified Energy Management (TEEM) for enabling more efficient engine designs. In: *2018 Joint Propulsion Conference, Cincinnati, OH, USA*. 2018:4798 (cit. on p. 5).

36. Meng X, Yang X, Chen M, and Zhu Z. High-level power extraction from adaptive cycle engine for directed energy weapon. In: *2018 Joint Propulsion Conference*. 2018:4518 (cit. on pp. 6, 33).

37. Corbett M. Shaft power extraction and waste heat rejection using a three stream variable cycle engine. SAE International Journal of Aerospace 2012;5:371 (cit. on pp. 6, 32).

38. Grönstedt T. Development of Methods for Analysis and Optimization of Complex Jet Engine Systems. PhD thesis. Gothenburg, Sweden: Chalmers University of Technology, 2000:33–4, 95–116 (cit. on pp. 6, 19, 20, 22, 31).

39. Simmons RJ. Design and Control of a Variable Geometry Turbofan with an Independently Modulated Third Stream. PhD thesis. Columbus, OH: The Ohio State University, 2009 (cit. on pp. 6, 25, 33).

40. Zheng J, Tang H, and Chen M. Optimal Matching Control Schedule Research on an Energy System. Energy Procedia 2019;158:1685–93 (cit. on p. 6).

41. Xu Z, Liu X, Chen M, Tang H, and Zhang J. Comprehensive Flow Path Design Method for the Adaptive Cycle Engine Considering the Coupling Relation of Multiple Components. Journal of Engineering for Gas Turbines and Power 2024;146 (cit. on p. 6).

42. Assato M, Inceer AA, Moraes L, Tomita J, Bringhenti C, Bravo-Mosquera P, Rosell D, and Grönstedt T. Performance Benefits of a Fan on Blade - FLADE - for a Variable Cycle Engine. In: *33rd Congress of the International Council of the Aeronautical Sciences (ICAS 2022)*. Vol. 7. Bonn, Germany: Deutsche Gesellschaft für Luft- und Raumfahrt, 2022:4888–902 (cit. on pp. 6, 32, 57).

43. Inceer AA. Low Bypass Ratio Variable Cycle Engine Concepts for High Speed Aircraft. MA thesis. Gothenburg, Sweden: Chalmers University of Technology, 2022 (cit. on p. 6).

44. Zhou H, Gao X, Wang Z, and Zhang W. The Transient Performance of FLADE Variable Cycle Engine During Mode Transition. In: *The Proceedings of the 2018 Asia-Pacific International Symposium on Aerospace Technology (APISAT 2018)*. Springer. Singapore, 2019:1685–95. DOI: 10.1007/978-981-13-3305-7_135 (cit. on pp. 6, 32).

45. Zhang X and Wang Z. Optimization of Flade Variable Cycle Engine Performance Based on Improved Differential Evolution Algorithm. In: *Gas Turbine India Conference*. Vol. 58509. American Society of Mechanical Engineers. 2017:1–10. DOI: 10.1115/GTINDIA2017-4771 (cit. on p. 6).

46. Bezborodova K and Filinov E. Double Bypass Turbojet Engine Analysis. In: *2021 International Scientific and Technical Engine Conference (EC)*. Springer. Singapore, 2019:1–5. DOI: 10.1109/EC52789.2021.10016815 (cit. on p. 6).

47. Grönstedt T, Au D, Kyprianidis K, and Ogaji S. Low-Pressure System Component Advancements and Its Influence on Future Turbofan Engine Emissions. American Society of Mechanical Engineers, Paper GT2009-60201. 2010. DOI: 10.1115/GT2009-60201 (cit. on p. 7).

48. Koff BL. Designing for fighter engine transients. In: *AGARD conference proceedings*. 324. 1983:2.1–2.15 (cit. on p. 7).

49. Mattingly JD, Heiser WH, and Pratt DT. Aircraft Engine Design. In: 2nd ed. AIAA Education Series. edited by J.S.Przemieniecki. Reston, NV: AIAA, 2002:3, 16, 17, 36–7, 112, 121, 123, 140, 172, 189, 193–5, 199–203, 341, 462, 465, 478, 525–6, 537–46. DOI: 10.2514/4.861444 (cit. on pp. 8, 10, 16, 17, 22, 24–27, 29, 30).

50. Jaw LC and Mattingly JD. Aircraft Engine Controls : Design, System Analysis, and Health Monitoring. In: AIAA Education Series. edited by J.A.Schetz. Reston, VA: AIAA, 2009:136–7, 155–8, 304–5, 324–7 (cit. on pp. 8, 29, 30).

51. Rosell D, Grönstedt T, Bravo-Mosquera PD, and Martini-Catalano F. Low BPR Turbofan Performance with Power Extraction. In: *33rd Congress of the International Council of the Aeronautical Sciences (ICAS 2022)*. Vol. 6. Bonn, Germany: Deutsche Gesellschaft für Luft- und Raumfahrt, 2022:4382–97 (cit. on pp. 8–11, 26, 37, 38).

52. Raymer D. Aircraft Design: A Conceptual Approach. In: 6th ed. AIAA Education Series. edited by J.A.Schetz. AIAA, 2018:36, 287, 396, 400, 416–22, 436–9, 446–51, 637, 639, 643, 662, 664, 667, 719. DOI: 10.2514/4.104909 (cit. on pp. 8, 11–14, 16, 23, 24).

53. Nicolai LM and Carichner GE. Fundamentals of aircraft and airship design, Volume 1–Aircraft Design. American Institute of Aeronautics and Astronautics, 2010 (cit. on pp. 8, 11, 13, 14, 16).

54. Jobe CE. Prediction and Verification of Aerodynamic Drag Part I: Prediction. In: *Thrust and drag: Its Prediction and Verification*. Ed. by Covert EE. Vol. 98. AIAA, 1985:131–3, 137–53 (cit. on pp. 8, 13, 14, 16).

55. Rosell D and Grönstedt T. Design Considerations of Low Bypass Ratio Mixed Flow Turbofan Engines with Large Power Extraction. Fluids 2022;7:21 (cit. on pp. 9, 26, 28, 37, 40, 41).

56. Rosell D. Power Extraction in Military Aircraft. Licentiate Dissertation. Gothenburg, Sweden: Chalmers University of Technology, 2023 (cit. on pp. 10–12, 21, 26, 28, 29, 31, 37–45).

57. Ball RE. The fundamentals of aircraft combat survivability: analysis and design. American Institute of Aeronautics and Astronautics, 2003 (cit. on p. 11).

58. Karlsson A. Take-off and landing performance. SA105X-Flygteknik vt2013 2010 (cit. on p. 11).

59. White FM. Fluid Mechanics. 4th ed. McGraw-Hill Education, 1998:771 (cit. on p. 14).

60. Sears WR. On projectiles of minimum wave drag. Quarterly of Applied Mathematics 1947;4:361–6 (cit. on p. 14).

61. Schemensky RT. Development of an Empirically Based Computer Program to Predict the Aerodynamic Characteristics of Aircraft. Volume II. Program User Guide. Tech. rep. General Dynamics Corporation, Convair Aerospace Division, Fort Worth, Texas, 1973 (cit. on p. 16).

62. Bravo-Mosquera PD, Abdalla AM, Cerón-Muñoz HD, and Catalano FM. Integration assessment of conceptual design and intake aerodynamics of a non-conventional air-to-ground fighter aircraft. Aerospace Science and Technology 2019;86:497–519 (cit. on p. 16).

63. Lowry JG and Polhamus EC. A Method for Predicting Lift Increments Due to Flap Deflection at Low Angles of Attack in Incompressible Flow. NACA TN-3911. 1957 (cit. on p. 16).

64. Gudmundsson S. General Aviation Aircraft Design: Applied Methods and Procedures. In: Oxford, UK: Butterworth-Heinemann, 2014:345–7 (cit. on p. 16).

65. Saravanamuttoo H. Steady and Transient Performance Prediction of Gas Turbine Engines. Tech. rep. AGARD-LS-183, 1992:1.1–1.18 (cit. on p. 19).

66. Benner P, Bollhöfer M, Kressner D, Mehl C, and Stykel T. Numerical algebra, matrix theory, differential-algebraic equations and control theory. Springer, 2015:ix, 463 (cit. on p. 19).

67. Campbell SL, Linh VH, and Petzold LR. Differential-algebraic equations. Scholarpedia 2008;3:2849 (cit. on p. 19).

68. Ascher UM and Petzold LR. Computer methods for ordinary differential equations and differential-algebraic equations. Vol. 61. Siam, 1998:12 (cit. on p. 19).

69. Grönstedt T. Advanced solvers for general high performance transient gas turbine simulation tools. In: *14th International Symposium on Air Breathing Engines, Florence, Italy*. 1999 (cit. on pp. 19, 20).

70. Petzold LR. Numerical methods for differential-algebraic equations: Current status and future directions. In: *Institute of Mathematics and its applications: conference on computational ordinary differential equations*. Lawrence Livermore National Lab. (LLNL), Livermore, CA (United States). 1989 (cit. on p. 19).

71. Campbell S, Ilchmann A, Mehrmann V, Reis T, et al. Applications of differential-algebraic equations: examples and benchmarks. Springer, 2019 (cit. on p. 19).

72. Press WH, Vetterling WT, Teukolsky SA, and Flannery BP. Numerical Recipes in FORTRAN: The Art of Scientific Computing. Cambridge University Press Cambridge UK, 1992 (cit. on p. 20).

73. Broyden CG. A class of methods for solving nonlinear simultaneous equations. Mathematics of computation 1965;19:577–93 (cit. on p. 20).

74. Broyden C. A new method of solving nonlinear simultaneous equations. The Computer Journal 1969;12:94–9 (cit. on p. 20).

75. Gordon S and McBride BJ. Computer Program for Calculation of Complex Chemical Equilibrium Compositions and Applications. NASA RP-1311. 1994 (cit. on p. 20).

76. ARP755B S. Aircraft Propulsion System Performance Station Designation and Nomenclature. SAE ARP755 Rev. B 1994 (cit. on p. 20).

77. Rosell D and Grönstedt T. Aircraft Performance Impact with a Turbofan Engine Using a Fan on Blade. Journal of Propulsion and Power 2026;42:392–406 (cit. on pp. 21, 24–26, 28, 30–34, 47–52).

78. Stenfelt M. On model based aero engine diagnostics. Licentiate Dissertation. Mälardalens universitet, 2023:29–30 (cit. on p. 22).

79. Rooney EC. Thrust-Drag Accounting Methodology. In: *Thrust and drag: Its Prediction and Verification*. Ed. by Covert EE. Vol. 98. AIAA, 1985:38–45 (cit. on p. 22).

80. Seddon J and Goldsmith EL. Intake Aerodynamics. In: 1st ed. AIAA Education Series. edited by J.S.Przemieniecki. New York: AIAA, 1985:12, 61–2, 81–9, 105–6, 170–1, 217–20, 236, 240–3, 268–9, 357 (cit. on pp. 22–25).

81. Mount JS. Effect of Inlet Additive Drag on Aircraft Performance. Journal of Aircraft 1965;2:374–8 (cit. on pp. 22, 24).

82. Hunt B and Gowadia N. Determination of Thrust and Throttle-Dependent Drag for Fighter Aircraft. In: *Aircraft Systems and Technology Conference*. 1981:1692. DOI: 10.2514/6.1981-1692 (cit. on p. 22).

83. Denner B, McCallum B, and Truax P. CFD Prediction of Inlet Spill Drag Increments. In: *34th AIAA/ASME/SAE/ASEE Joint Propulsion Conference and Exhibit*. 1998:3566. DOI: 10.2514/6.1998-3566 (cit. on p. 22).

84. Evans AB. The effects of compressor seventh-stage bleed air extraction on performance of the F100-PW-220 afterburning turbofan engine. NASA CR-179447. 1991 (cit. on p. 22).

85. Farokhi S. Aircraft Propulsion. In: 2nd ed. Chichester, United Kingdom: John Wiley & Sons Ltd, 2014:8–9, 359 (cit. on pp. 23, 27).

86. Anderson JD. One-Dimensional Flow with Friction. In: *Modern Compressible Flow: with Historical Perspective*. 3rd ed. New York, NY: McGraw-Hill, 2004:111–7 (cit. on pp. 23, 33).

87. El-Sayed AF and Emeara MS. Intake of aero-engines: a case study. In: *The international conference of engineering sciences & applications (ICESA)*. Coalesce Research Group Aswan, Egypt. 2016:301–9 (cit. on p. 24).

88. Williams M and Stevens K. Computational prediction of subsonic intake spillage drag. AIAA paper 2006-3871 2006 (cit. on p. 24).

89. Vdoviak JW, Knott PR, and Ebacker JJ. Aerodynamic/Acoustic Performance of YJ101/Double Bypass VCE with Coannular Plug Nozzle. NASA CR-159869. 1981 (cit. on pp. 25, 34).

90. Szeliga R and Allan R. Advanced Supersonic Technology Propulsion System Study. NASA CR-143634. 1974 (cit. on pp. 25, 47).

91. Matuschek T, Otten T, Zenkner S, Becker RG, Zamboni J, and Moerland E. Application of a Multidisciplinary Design Process to Assess the Influence of Requirements and Constraints on the Design of Military Engines. Journal of Engineering for Gas Turbines and Power 2024;146:4–5 (cit. on pp. 26, 31).

92. Yuhas A and Ray R. Effects of Bleed Air Extraction of Thrust Levels on the F404-GE-400 Turbofan Engine. AIAA Paper 1992–3092. 1992. DOI: 10.2514/6.1992-3092 (cit. on p. 27).

93. Grieb H. Projektierung von Turboflugtriebverken. In: 1st ed. Basel, Switzerland: Birkhäuser, 2004:156, 160, 170, 185–8, 200–3, 562–4, 735. DOI: 10.1007/978-3-0348-7938-5 (cit. on pp. 27, 29, 31).

94. Nadon LJ, Kramer SC, and King PI. Multidisciplinary optimization in conceptual design of mixed-stream turbofan engines. Journal of propulsion and power 1999;15:17–22 (cit. on p. 27).

95. Mattingly J and Heiser W. Performance estimation of the mixed flow, afterburning, cooled, two-spool turbofan engine with bleed and power extraction. In: *22nd Joint Propulsion Conference*. 1986:1757 (cit. on p. 27).

96. Mattingly J. Performance estimation of some variable bypass ratio turbofan engines. In: *34th AIAA/ASME/SAE/ASEE Joint Propulsion Conference and Exhibit*. 1998:3894 (cit. on pp. 27, 29).

97. Koff BL. Gas Turbine Technology Evolution: A Designers Perspective. Journal of Propulsion and Power 2004;20:577–95 (cit. on pp. 27, 31).

98. Guha A. Optimum fan pressure ratio for bypass engines with separate or mixed exhaust streams. Journal of Propulsion and Power 2001;17:1117–22 (cit. on p. 28).

99. Aziz M, Owis FM, and Abdelrahman M. Preliminary design of a transonic fan for a low by-pass turbofan engine. International Review of Aerospace Engineering 2013;6:114–27 (cit. on p. 29).

100. Walsh P and Fletcher P. Gas Turbine Performance. In: 2nd ed. Oxford, United Kingdom: Blackwell Science Ltd, 2004:226. DOI: 10.1002/9780470774533 (cit. on p. 29).

101. Mattingly J. Easy method of matching fighter engine to airframe for use in aircraft engine design courses. In: *25th Joint Propulsion Conference*. 1989:2260 (cit. on p. 29).

102. Langton R and MacIsaac B. Gas turbine propulsion systems. John Wiley & Sons, 2011:63–5, 184–6 (cit. on pp. 30, 31).

103. Langston LS. Fahrenheit 3,600. mechanical engineering 2007;129:34–7 (cit. on p. 31).

104. Oates GC. Aircraft Propulsion Systems Technology and Design. In: AIAA Education Series. edited by J.S.Przemieniecki. Washington, DC: AIAA, 1989:7, 8, 50, 64 (cit. on p. 31).

105. Ehrlich H, Kurz K, Rued K, and Lauer W. Trends in Military Aeroengine-Design—From EJ200 to Future Manned and Unmanned Vehicle Propulsion. AIAA paper 2003-2612. 2003. DOI: 10.2514/6.2003-2612 (cit. on p. 31).

106. Thomas WW and Sprunger EV. Two-Spool Variable Cycle Engine. US Patent 4,043,121. 1977 (cit. on pp. 31, 33).

107. Johnson JE. Spillage Drag and Infrared Reducing FLADE Engine. US Patent 5,404,713. 1995 (cit. on pp. 31, 32).

108. Wadia AR, Turner AG, Dziech AM, Szucs PN, and Decker JJ. FLADE Fan with Different Inner and Outer Airfoil Stagger Angles at a Shroud Therebetween. US Patent 7,758,303. 2010 (cit. on p. 31).

109. Buettner RW. Dynamic Modeling and Simulation of a Variable Cycle Turbofan Engine with Controls. PhD thesis. Dayton, OH: Wright State University, 2017:1–2 (cit. on p. 32).

110. Sigthorsson D, Oppenheimer MW, and Doman DB. Aircraft Thermal Endurance Optimization Part I: Using A Mixed Dual Tank Topology And Robust Temperature Regulation. In: *AIAA Scitech 2019 Forum*. AIAA, 2019. DOI: 10.2514/6.2019-1662. eprint: https://arc.aiaa.org/doi/pdf/10.2514/6.2019-1662 (cit. on p. 32).

111. Johnson JE. Adaptive Engine. US Patent US2011/0167792 A1. 2011 (cit. on p. 32).

112. Howlett R. Advanced Supersonic Propulsion Study, Phase 2. NASA CR-134904. 1975 (cit. on p. 32).

113. Brown RH. Integration of a Variable Cycle Engine Concept in a Supersonic Cruise Aircraft. AIAA Paper 1978–1049. 1978. DOI: 10.2514/6.1978-1049 (cit. on p. 32).

114. Zheng J, Tang H, Chen M, and Yin FJ. Equilibrium Running Principle Analysis on an Adaptive Cycle Engine. Applied Thermal Engineering 2018;132:393–409 (cit. on p. 32).

115. Zhang J, Dong P, Tang H, Zheng J, Wang J, and Chen M. General Design Method of Control Law for Adaptive Cycle Engine Mode Transition. AIAA Journal 2022;60:330–44 (cit. on p. 32).

116. Zhang J, Tang H, and Chen M. Robust Design of an Adaptive Cycle Engine Performance Under Component Performance Uncertainty. Aerospace Science and Technology 2021;113:1–21 (cit. on p. 32).

117. Muir DE, Saravanamuttoo HI, and Marshall D. Health Monitoring of Variable Geometry Gas Turbines for the Canadian Navy. Journal of Engineering for Gas Turbines and Power 1989;111:244–50 (cit. on p. 33).

118. Sirinoglou AA. Implementation of Variable Geometry for Gas Turbine Performance Simulation Turbomatch Improvement. MA thesis. Cranfield, United Kingdom: Cranfield Institute of Technology, 1992 (cit. on p. 33).

119. Yueliu Z and Yuan W. Analysis of Aerodynamic Design Characteristics of Flade Fan. Procedia Engineering 2015;99:723–33 (cit. on p. 33).

120. Li P, Zuo Z, Li J, Tao H, Guo W, and Chen H. Characteristics of inlet guide vane adjustment of multi-stage axial compressor in compressed air energy storage system. Journal of Energy Storage 2023;72:2 (cit. on p. 33).

121. Ma S, Zhang X, Wang Z, and Jiang T. Modeling, Simulation and Performance Comparison of Variable Cycle Engine based on Object-Oriented. In: *2023 23rd International Conference on Control, Automation and Systems (ICCAS)*. IEEE. 2023:189–95. DOI: 10.23919/ICCAS59377.2023.10317024 (cit. on p. 33).

122. Grönstedt T, Au D, Kyprianidis K, and Ogaji S. Low-Pressure System Component Advancements and its Influence on Future Turbofan Engine Emissions. In: *Turbo Expo: Power for Land, Sea, and Air*. Vol. 48852. 2009:505–16. DOI: 10.1115/GT2009-60201 (cit. on p. 35).

123. Lolis P. Development of a Preliminary Weight Estimation Method for Advanced Turbofan Engines. PhD thesis. Cranfield, United Kingdom: Cranfield University, 2014 (cit. on p. 35).

124. Thoma EM, Grönstedt T, and Zhao X. Quantifying the environmental design trades for a state-of-the-art turbofan engine. Aerospace 2020;7:148 (cit. on p. 35).

125. Drego A. Harnessing the Complexity for Vehicle System Design at the Concept Design Phase of an Aircraft. Proceedings of the Design Society 2022;2:1845–54 (cit. on p. 47).

126. Youssef M. On Modelling a Fighter Aircraft Fuel System as a Heat Sink. MA thesis. Linköping, Sweden: Linköping University, 2023 (cit. on p. 47).

127. Drego AD, Andersson D, and Staack I. Parameter Tuning of a Vapor Cycle System for a Surveillance Aircraft. Aerospace 2024;11:1–2 (cit. on p. 47).